J. Fluid Mech. (2003), *vol.* 483, *pp.* 129–163.
DOI: 10.1017/S0022112003004208 Printed in the United Kingdom

Scattered and free waves over periodic beds

By R. PORTER[1] AND D. PORTER[2]

[1]School of Mathematics, University of Bristol, Bristol BS8 1TW, UK

[2]Department of Mathematics, The University of Reading, P. O. Box 220, Whiteknights, Reading RG6 6AX, UK

(Received 17 December 2001 and in revised form 6 May 2002)

The behaviour of water waves over periodic beds is considered in a two-dimensional context and using linear theory. Three cases are investigated: the scattering of waves by a finite section of periodic topography; the Bloch problem for infinite periodic topography; and sloshing motions over periodic topography confined between vertical boundaries. Connections are established between these problems.

A transfer matrix method incorporating evanescent modes is developed for the scattering problem, which reduces the computation to that required for a single period, without compromising full linear theory. The problem of the existence of Bloch waves can also be posed on a single period, leading to a close relationship between it and the scattering problem. Sloshing motions over periodic beds, which may be regarded as special cases of the Bloch problem, are also found to have a significant connection with wave scattering.

Integral equations methods allied to the Galerkin approximation are used to resolve the three problems numerically. In particular, the full linear solution for Bragg resonance is presented, allowing the accuracy of existing approximations to this phenomenon to be assessed. The selection of results given illustrates the main features of the work.

1. Introduction

This paper investigates the interactions between surface water waves and periodic bedforms in three different situations. One of these is the scattering of given incident waves by finitely many periods of topography. The other two, in contrast, concern the existence of unforced waves over periodically varying beds, of infinite and finite extent.

The two-dimensional scattering of water waves by a finite number of periodic ripples, or sandbars, on an otherwise horizontal, flat bed has been a subject of investigation for many years. Interest centres on the existence of a phenomenon which is usually referred to as Bragg resonance, terminology carried over from a parallel effect in crystallography. In the water wave context, this effect produces reflection of a substantial fraction of the incident wave energy when the wavelength of the incoming wave is about twice the wavelength of the ripples, even when the ripple amplitude is a small fraction of the mean undisturbed water depth. This resonant reflection was captured in wavetank experiments carried out by Davies & Heathershaw (1984), triggering a number of papers in which the authors sought to develop a variety of mathematical models of ripple bed scattering consistent with the experimental values.

The perturbation approach used by Davies (1982) to examine wave propagation over a ripple bed breaks down at resonance, as noted by Mei (1985) who presented a first-order theory which does indeed account for the expected significant reflected energy. Miles (1998) has recently derived a solution in the form of an expansion, valid at resonance, which also agrees well with the measurements of Davies & Heathershaw (1984).

The mild-slope equation, which results from approximating the vertical structure of the fluid motion and was first derived independently by Berkhoff (1973, 1976) and Smith & Sprinks (1975), was found to give an inadequate description of Bragg resonance. Modifications introduced by Kirby (1986), Massel (1993) and Chamberlain & Porter (1995*a*) remedy this deficiency in the original equation and lead to computational results which closely match those found experimentally. In the long-wave limit, the mild-slope equation reduces to the shallow-water equation, used by Davies, Guazzelli & Belzons (1989) to investigate Bragg resonance. In this setting, the free-surface elevation over a ripple bed of small amplitude satisfies the Mathieu equation and resonance is determined by the associated stability theory.

A different approach to modelling Bragg resonance involves piecewise constant discretizations of the topography, the individual scattering properties of adjacent intervals being coupled through transfer or transition matrices to form the corresponding properties for the whole ripple bed. The basic idea, described by Devillard, Dunlop & Souillard (1988), was used by O'Hare & Davies (1992, 1993) and, in a modified form involving two levels of bed approximation, by Rey (1992) and Guazzelli, Rey & Belzons (1992). In particular, those authors examined the critical relationship between the bed discretization step length and the retention of evanescent wave modes in the coupling process between adjoining intervals. A theory applicable to certain waveguide problems which also uses transfer matrices incorporating evanescent modes on uniform sections of the guide can be found in Collin (1991).

We return to the problem of Bragg resonance in this paper and, apparently for the first time, present a solution based on full linear water wave theory, without approximation. To achieve this, we make use of a technique recently devised by Porter & Porter (2000) for calculating two-dimensional wave scattering over arbitrary bedforms. However, we do not implement the earlier method directly for the whole ripple bed, because of the computational cost which would be incurred to achieve high resolution, even for a moderate number of ripples. Instead, we develop a procedure in which the scattering properties of an extended bedform may be constructed in a piecemeal fashion, without compromising full linear theory. Although this method can be applied to general topography, it is ideally suited to ripple beds, where the effect of a repeated bed section leads to computational efficiency and reveals a certain structure. The approach consists of defining 'incoming' and 'outgoing' states for an isolated section of topography, a single period in the present application. These states, which contain information about finitely many evanescent modes in addition to propagating waves, are determined by solving a local problem for a single period, using the integral equation method of Porter & Porter (2000). The scattering properties for an arbitrary number of periods of the ripple bed may be deduced from those for the single period through a transfer matrix technique. Although reminiscent of stepwise bed approximations in its use of transfer matrices to combine sections of topography, the present approach differs significantly from earlier work by using the full linear solutions for the component bedforms. As a result, the method yields the exact solution for ripple bed scattering to arbitrary accuracy, within the framework

of linearized theory. The 'wide-spacing' approximation to scattering, a special case of the formulation that we give, is briefly considered and a particular feature is inferred which proves to have significance in the unapproximated solution.

The procedure outlined requires that an extended version of the scattering problem, incorporating evanescent modes, be solved for a single period of the topography. In addition to the computational saving achieved, there is a further motivation for developing the technique: the so-called Bloch wave problem may also be reduced to one posed on a single period of the bedform.

This different problem investigates the existence of unforced waves over a periodic bed of *infinite* extent and it is therefore an eigenvalue problem. Bloch waves have been widely studied in the area of solid-state physics, in relation to particle motion through a periodic potential field (see, for example, Ashcroft & Mermin 1976). In the context of water waves, Bloch theory has been used by Chou (1998), who considered wave propagation in the presence of a variety of infinite, periodic arrays of scatterers lying in the fluid surface. More recently, McIver (2001) has examined water wave behaviour in periodic arrays of vertical cylinders that extend throughout the fluid depth.

By using Bloch's theorem, the present investigation of wave propagation over an infinite periodic bed may be reduced to an eigenvalue problem for a single period. Although it is therefore posed on the same domain as the extended scattering problem described earlier, the two problems otherwise appear to have little in common.

We can, however, pose an extended form of the Bloch problem and, in addition to seeking those eigenvalues which lead to propagating waves over the infinite periodic bedform, we may also seek eigenvalues corresponding to evanescent waves, which amplify or diminish as they cross a single period. Such localized solutions do not extend to the infinite domain and are not Bloch waves. However, they do relate to the extended scattering problem, which *is* concerned with the behaviour of evanescent modes on a period of topography. The connection between the two situations is made explicit by showing that the eigenvalues of the extended transfer matrix used in the scattering case approximate those of the extended Bloch problem. In particular, the eigenvalues of the lowest-order transfer matrix, corresponding to the wide-spacing approach, are approximations to the eigenvalues of the original Bloch wave problem. The interplay between the two problems can be exploited by using the Bloch problem to formulate an alternative version of the transfer matrix. By this means, the solution of the scattering problem can in principle be deduced from that of the Bloch problem and, conversely, the Bloch eigenvalues can be deduced from the extended scattering problem. The Bloch problem is resolved by converting it into both a single integral equation and a pair of coupled integral equations, each of the formulations playing a useful role in the solution process.

The final aspect of this investigation addresses another eigenvalue problem, namely, the existence of 'sloshing modes' over a finite section of a periodic bed. This situation may be regarded as a special case of the conventional Bloch wave problem, in which the periodic boundary conditions are reduced to those of Neumann or Dirichlet type. Thus, the relationship between the scattering and Bloch problems alluded to above extends to embrace the sloshing wave problem. In particular, we deduce that the frequency band in which Bragg scattering occurs is bounded by the sloshing frequencies for a single period of the topography confined between vertical walls.

Thus, close connections are established between the three problems considered. These are illustrated by a selection of numerical results, which are determined by using Galerkin's method to approximate the solutions of the integral equations that arise.

Following the presentation of the overall formulation of the three problems in § 2, the details of the scattering problem and the unforced wave problems are pursued in §§ 3 and 4, respectively. Section 5 is devoted to a description of the numerical techniques employed and the resulting solutions.

2. Formulation

We use Cartesian coordinates (x, y), arranged so that y is measured vertically downwards and $y = 0$ coincides with the undisturbed free surface of the fluid. The bed is given by $y = H_L(x)$ for $-\infty < x < \infty$, where

$$H_L(x) = \begin{cases} h_1, & x < 0 \quad \text{and} \quad L < x, \\ h(x), & 0 \leqslant x \leqslant L, \end{cases} \tag{2.1}$$

h_1 being a constant. The function $h(x) > 0$ is assumed to be continuous for $0 \leqslant x \leqslant L$, with $h(0) = h(L) = h_1$ and it has continuous derivative for $0 < x < L$. We further suppose that $h(x)$ is periodic with period ℓ and set $L = N\ell$, where $N = 1, 2, \ldots$. Therefore

$$h(x + n\ell) = h(x), \quad n = 0, 1, \ldots, N-1, \quad 0 \leqslant x \leqslant \ell,$$

where $h(0) = h(\ell)$ ensures the required continuity.

We shall construct the solution for an arbitrary value of N from that for $N = 1$ and therefore concentrate on the problem for a single period of the bed with ℓ replacing L in (2.1).

On the basis of linear water wave theory, the velocity potential Φ which describes the fluid motion can be written as

$$\Phi(x, y, t) = \mathrm{Re}\{\phi(x, y)\mathrm{e}^{-\mathrm{i}\omega t}\},$$

where ϕ satisfies

$$\nabla^2\phi \equiv \phi_{xx} + \phi_{yy} = 0 \qquad \text{in } D\colon -\infty < x < \infty,\ 0 < y < H_\ell(x), \tag{2.2}$$

$$\phi_y + K\phi = 0 \qquad \text{on } y = 0,\ -\infty < x < \infty, \tag{2.3}$$

with $K = \omega^2/g$ (g is acceleration due to gravity), and

$$\phi_n = 0 \qquad \text{on } y = H_\ell(x),\ -\infty < x < \infty, \tag{2.4}$$

the subscript n denoting the outward normal derivative from D on $y = H_\ell(x)$. The points $(0, h_1)$, (ℓ, h_1) are to be excluded from (2.4) if H_ℓ is not differentiable there.

We also have to specify the behaviour of ϕ for $x < 0$ and $x > \ell$ and to this end we note that separation solutions of (2.2) corresponding to a horizontal bed at $y = h_i$ (a notation which anticipates the need to make use of a further depth h_2 later) are

$$\mathrm{e}^{\pm k_{i,n}x}\psi_{i,n}(y), \quad n = 0, 1, 2, \ldots,$$

where

$$\left.\begin{aligned} \psi_{i,n}(y) &= N_{i,n}^{-1/2}\cos k_{i,n}(h_i - y), \\ N_{i,n} &= \tfrac{1}{2}\{1 + \sin(2k_{i,n}h_i)/2k_{i,n}h_i\}, \end{aligned}\right\} \quad n = 0, 1, 2, \ldots.$$

We have used $k_{i,n}$ ($n = 1, 2, \ldots$) to denote the positive real roots of

$$K = -k_{i,n}\tan k_{i,n}h_i,$$

arranged so that $k_{i,n} < k_{i,n+1}$, whilst $k_{i,0} = -\mathrm{i}k_i$ corresponds to the propagating wave solutions

$$\mathrm{e}^{\mp \mathrm{i}k_i x}\psi_{i,0}(y) \equiv N_{i,0}^{-1/2}\mathrm{e}^{\mp \mathrm{i}k_i x}\cosh k_i(h_i - y),$$

k_i being the positive real root of the dispersion relation

$$K = k_i \tanh k_i h_i .$$

The set $\{\psi_{i,n}\}$ is orthonormal on the interval $[0, h_i]$ with weight h_i^{-1}, so that

$$\int_0^{h_i} \psi_{i,n}(y)\psi_{i,m}(y)\,\mathrm{d}y = h_i\delta_{mn}, \qquad n, m = 0, 1, 2, \ldots,$$

and it is complete.

As indicated earlier, our aim is to construct the solution for an arbitrary number of periods of the topography in terms of that for a single period. We therefore need to identify 'input' and 'output' states for a single, typical period in a larger array, which we locate on $0 \leqslant x \leqslant \ell$ for convenience. We do this by defining a local problem in which (2.2), (2.3) and (2.4) hold for $-X \leqslant x \leqslant \ell + X$, where $X > 0$, together with

$$\begin{aligned}\phi(x, y) &\sim -\sum_{n=0}^{M}\{A_n^-\mathrm{e}^{-k_{1,n}x} + B_n^-\mathrm{e}^{k_{1,n}x}\}\psi_{1,n}(y), \qquad x \sim -X,\\ &\sim \sum_{n=0}^{M}\left\{A_n^+\mathrm{e}^{k_{1,n}(x-\ell)} + B_n^+\mathrm{e}^{-k_{1,n}(x-\ell)}\right\}\psi_{1,n}(y), \qquad x \sim \ell + X. \end{aligned} \tag{2.5}$$

We therefore include $M \geqslant 0$ non-propagating modes in the coupling between adjacent periods; the coupling with $M = 0$ is the familiar wide-spacing construction. In effect, we treat the first $M + 1$ modes of the solution over the sections of flat bed as propagating modes for the purpose of linking periods of topography. Numerical calculations will determine the value of M required to give a specified accuracy in the coupling process.

We respectively represent the 'incoming' and 'outgoing' states for the problem over a single period of topography by $\boldsymbol{A}^-$ and $\boldsymbol{B}^-$ for $x \leqslant 0$ and $\boldsymbol{A}^+$ and $\boldsymbol{B}^+$ for $x \geqslant \ell$, where

$$\boldsymbol{A}^\pm = (A_0^\pm, \ldots, A_M^\pm)^{\mathrm{T}}, \quad \boldsymbol{B}^\pm = (B_0^\pm, \ldots, B_M^\pm)^{\mathrm{T}}. \tag{2.6}$$

These may be related both through an extended scattering matrix $\mathscr{S}$, which transforms the incoming states into the outgoing states, and an extended transfer matrix $\mathscr{P}$, which relates the corresponding states on the left and right of the varying topography. The appropriate definitions are

$$\begin{pmatrix}\boldsymbol{B}^-\\ \boldsymbol{B}^+\end{pmatrix} = \mathscr{S}\begin{pmatrix}\boldsymbol{A}^-\\ \boldsymbol{A}^+\end{pmatrix}, \qquad \begin{pmatrix}\boldsymbol{B}^+\\ \boldsymbol{A}^+\end{pmatrix} = -\mathscr{P}\begin{pmatrix}\boldsymbol{A}^-\\ \boldsymbol{B}^-\end{pmatrix}. \tag{2.7}$$

With $M = 0$ these are the usual 2×2 scattering and transfer matrix couplings between the amplitudes of the propagating waves, except for the minus sign which has been introduced into $\mathscr{P}$ for algebraic convenience.

We also need to introduce the extended scattering matrix $\mathscr{S}_N$ and the extended transfer matrix $\mathscr{P}_N$ for N contiguous periods of the bedform. (The conventions $\mathscr{S} = \mathscr{S}_1$ and $\mathscr{P} = \mathscr{P}_1$ have been adopted for notational simplicity.) The parallel

definitions to (2.7) are

$$\begin{pmatrix} \boldsymbol{B}_0^- \\ \boldsymbol{B}_N^+ \end{pmatrix} = \mathscr{S}_N \begin{pmatrix} \boldsymbol{A}_0^- \\ \boldsymbol{A}_N^+ \end{pmatrix}, \qquad \begin{pmatrix} \boldsymbol{B}_N^+ \\ \boldsymbol{A}_N^+ \end{pmatrix} = -\mathscr{P}_N \begin{pmatrix} \boldsymbol{A}_0^- \\ \boldsymbol{B}_0^- \end{pmatrix}, \tag{2.8}$$

where the subscripts 0 and N denote the states at the boundaries of the whole of the varying topography, at $x = 0$ and $x = L = N\ell$, respectively.

Now $\mathscr{P}$ represents the transfer across each component period, provided that (2.5) is modified to allow for translations in x. It follows by matching the incoming and outgoing states at the interfaces between adjacent periods that

$$\mathscr{P}_N = \mathscr{P}^N = \begin{pmatrix} P_{11} & P_{12} \\ P_{21} & P_{22} \end{pmatrix}, \tag{2.9}$$

where the partitioning into $(M+1)\times(M+1)$ matrices P_{ij} for $i, j = 1, 2$ allows us to deduce from (2.8) that

$$\mathscr{S}_N = \begin{pmatrix} -P_{22}^{-1}P_{21} & -P_{22}^{-1} \\ P_{12}P_{22}^{-1}P_{21} - P_{11} & P_{12}P_{22}^{-1} \end{pmatrix}. \tag{2.10}$$

Our aim is to determine the scattering properties of the complete ripple bed, which are embedded in the extended scattering matrix $\mathscr{S}_N$, and to extricate them we must introduce radiation conditions for the scattering process as a whole. Again using the subscript N to identify the overall problem, we require

$$\begin{aligned} \phi_N(x, y) &\sim -\{A^- \mathrm{e}^{\mathrm{i}k_1 x} + B^- \mathrm{e}^{-\mathrm{i}k_1 x}\}\psi_{1,0}(y), \qquad x \to -\infty, \\ &\sim \{A^+ \mathrm{e}^{-\mathrm{i}k_1(x-L)} + B^+ \mathrm{e}^{\mathrm{i}k_1(x-L)}\}\psi_{1,0}(y), \qquad x \to \infty, \end{aligned} \tag{2.11}$$

in which the incoming wave amplitudes $A^\pm$ are given and the outgoing wave amplitudes $B^\pm$ are to be determined. In terms of the usual reflection and transmission coefficients, denoted by $R^\pm$ and $T^\pm$ respectively for wavetrains incident from $x = \pm\infty$, we may write

$$\begin{pmatrix} B^- \\ B^+ \end{pmatrix} = \widehat{\mathscr{S}}_N \begin{pmatrix} A^- \\ A^+ \end{pmatrix}, \qquad \widehat{\mathscr{S}}_N = \begin{pmatrix} R^- & -T^+ \mathrm{e}^{\mathrm{i}k_1 L} \\ -T^- \mathrm{e}^{\mathrm{i}k_1 L} & R^+ \mathrm{e}^{2\mathrm{i}k_1 L} \end{pmatrix}, \tag{2.12}$$

in which $\widehat{\mathscr{S}}_N$ is the conventional scattering matrix for the complete problem.

To relate $\mathscr{S}_N$ and $\widehat{\mathscr{S}}_N$, we note that the 'incoming' states for the whole topography comprise only the incoming propagating modes in (2.11); the corresponding 'outgoing' states contain information about evanescent modes, as well as the outgoing propagating waves. Thus

$$\begin{aligned} \boldsymbol{A}_0^- &= (A^-, 0, \ldots, 0)^{\mathrm{T}}, \quad \boldsymbol{B}_0^- = (B^-, B_1^-, \ldots, B_M^-)^{\mathrm{T}}, \\ \boldsymbol{A}_N^+ &= (A^+, 0, \ldots, 0)^{\mathrm{T}}, \quad \boldsymbol{B}_N^+ = (B^+, B_1^+, \ldots, B_M^+)^{\mathrm{T}}, \end{aligned}$$

and we may now deduce from (2.8) and (2.12) that

$$\widehat{\mathscr{S}}_N = \mathscr{U}^{\mathrm{T}} \mathscr{S}_N \mathscr{U}, \qquad \mathscr{U} = \begin{pmatrix} \boldsymbol{U} & \boldsymbol{0} \\ \boldsymbol{0} & \boldsymbol{U} \end{pmatrix}, \tag{2.13}$$

where $\boldsymbol{U} = (1, 0, \ldots, 0)^{\mathrm{T}}$ and $\boldsymbol{0}$ is the null vector, both being of length $M+1$. This equation gives the required transformation of $\mathscr{S}_N$ into $\widehat{\mathscr{S}}_N$; it includes the special case $\mathscr{S}_N = \widehat{\mathscr{S}}_N$ for $M = 0$.

The standard scattering matrix $\widehat{\mathscr{S}}_N$ for N periods of topography can therefore be calculated, via (2.9), (2.10) and (2.13), from the transition matrix $\mathscr{P}$ for a single period, taking into account as many evanescent modes as we wish. This process is implemented in § 3.

We now examine a different situation which may also be restricted to an investigation on a single period, namely the so-called Bloch problem for wave propagation over a periodic bed of *infinite* extent. In this case (2.2), (2.3) and (2.4) remain in force but with the latter now holding on $y = h(x)$ for $-\infty < x < \infty$ where $h(x + n\ell) = h(x)$ for $0 \leqslant x \leqslant \ell$ and $n \in \mathbb{Z}$. As before, $h(0) = h(\ell) = h_1$ guarantees the continuity of $h(x)$. The periodicity allows us to restrict attention to the interval $0 \leqslant x \leqslant \ell$ if we make the Bloch assumption that a propagating wave, if it exists, is modified only by a change of phase as it crosses a single period of the bed. Thus we suppose that

$$\phi(x + n\ell, y) = \mathrm{e}^{\mathrm{i}n\beta\ell}\phi(x, y), \quad n \in \mathbb{Z}, \tag{2.14}$$

for some real β. An equivalent procedure which makes the propagating Bloch wave explicit is to invoke the Floquet (or Bloch) substitution

$$\phi(x, y) = \mathrm{e}^{\mathrm{i}\beta x}\chi(x, y),$$

in which $\chi(x, y)$ is required to be periodic in x with period ℓ.

It follows that the time-independent part of the velocity potential in the Bloch problem must satisfy

$$\left.\begin{aligned} \nabla^2\phi &= 0 \qquad \text{in } 0 < x < \ell,\ 0 < y < h(x), \\ \phi_y + K\phi &= 0 \qquad \text{on } y = 0,\ 0 \leqslant x \leqslant \ell, \\ \phi_n &= 0 \qquad \text{on } y = h(x),\ 0 \leqslant x \leqslant \ell, \end{aligned}\right\} \tag{2.15}$$

together with the coupled boundary conditions

$$\phi(\ell, y) = \mathrm{e}^{\mathrm{i}\beta\ell}\phi(0, y), \quad \phi_x(\ell, y) = \mathrm{e}^{\mathrm{i}\beta\ell}\phi_x(0, y), \quad 0 \leqslant y \leqslant h_1, \tag{2.16}$$

which follow from (2.14). Clearly, β plays the part of an eigenvalue parameter and we therefore seek values $\beta(K)$ (where $K = \omega^2/g$) for which there is a non-trivial solution ϕ of (3.12) and (2.16). This solution can be extended to all x by (2.14) and represents a Bloch wave propagating over the periodic bed in the positive x-direction, if $\beta(K) > 0$. The solution $\overline{\phi}$ corresponding to the eigenvalue $-\beta(K)$ represents the wave travelling in the opposite direction.

Having modified the scattering problem to incorporate non-propagating modes within a local framework, we also consider an extended form of the Bloch problem in which (2.16) is replaced by

$$\phi(\ell, y) = \mu\,\phi(0, y), \quad \phi_x(\ell, y) = \mu\,\phi_x(0, y), \quad 0 \leqslant y \leqslant h_1, \tag{2.17}$$

where $\mu(K) \in \mathbb{C}$ is now the eigenvalue parameter. This is also a local problem in the sense that only eigenvalues of the form $\mathrm{e}^{\mathrm{i}\beta\ell}$ for $\beta \in \mathbb{R}$ lead to Bloch waves which can be extended onto $-\infty < x < \infty$. Real eigenvalues represent an increase or decrease in the amplitude of non-propagating modes as they travel across a period of topography.

If the bed is symmetric, in the sense that $h(\ell - x) = h(x)$ for $0 \leqslant x \leqslant \ell$, the standard Bloch problem also incorporates, for particular values of $\beta \in \mathbb{R}$, the sloshing of a fluid between vertical walls containing a periodic bed of finite extent. This situation is considered in § 4 along with the extended Bloch problem.

3. The scattering problem

3.1. *Full linear theory*

We solve the local scattering problem comprising (2.2), (2.3) and (2.4), restricted to the domain for which $-X \leqslant x \leqslant X + \ell$, together with (2.5), by converting it to a system of integral equations. This approach allows us to take advantage of a related formulation given by Porter & Porter (2000) and we do not need to repeat details given in the earlier work.

The conversion requires the Green's function

$$G_i(x, y|x_0, y_0) = \sum_{n=0}^{\infty} \frac{\psi_{i,n}(y)\psi_{i,n}(y_0)}{2k_{i,n}h_i} \exp(-k_{i,n}|x - x_0|), \qquad (x, y) \neq (x_0, y_0), \tag{3.1}$$

for $i = 1, 2$ (h_2 will arise shortly) which satisfies

$$\nabla^2 G_i = -\delta(x - x_0)\delta(y - y_0) \quad \text{in } -\infty < x < \infty,\ 0 < y < h_i,$$

where $-\infty < x_0 < \infty$, $0 < y_0 < h_i$,

$$G_{i\,y} + KG_i = 0 \quad \text{on } y = 0,\ -\infty < x < \infty,$$

and

$$G_{i\,y} = 0 \quad \text{on } y = h_i,\ -\infty < x < \infty,$$

together with the radiation condition

$$G_i \sim \mathrm{i}\exp(\mp \mathrm{i}k_i x_0 + \mathrm{i}k_i|x|)\psi_{i,0}(y_0)\psi_{i,0}(y)/2k_i h_i, \quad x \to \pm\infty.$$

We also use Green's identity

$$\iint_{\mathscr{D}} (\phi\nabla^2 G - G\nabla^2\phi)\,\mathrm{d}x\,\mathrm{d}y = \int_{\partial\mathscr{D}} \left(\phi\frac{\partial G}{\partial n} - G\frac{\partial\phi}{\partial n}\right)\mathrm{d}s, \tag{3.2}$$

where $\partial\mathscr{D}$ denotes the boundary of $\mathscr{D}$, s measures the arc length on $\partial\mathscr{D}$ and $\partial/\partial n$ is the outward normal derivative from $\mathscr{D}$ on $\partial\mathscr{D}$.

In particular, if we apply (3.2) to the subdomain of $\mathscr{D}$ bounded laterally by $x = -X$ and $x = 0$ with $G = G_1(x, y|x_0, y_0) + G_1(-x, y|x_0, y_0)$, we obtain

$$\phi(x_0, y_0) = -\sum_{n=0}^{M} A_n^- \{\exp(-k_{1,n}x_0) + \exp(k_{1,n}x_0)\}\psi_{1,n}(y_0) + \int_0^{h_1} 2G_1(0, y|x_0, y_0)\phi_x(0, y)\,\mathrm{d}y, \tag{3.3}$$

for $-X \leqslant x_0 \leqslant 0$. Discarding all but the first $M+1$ modes as $x_0 \to -X$, in accordance with (2.5), we find that

$$B_n^- = A_n^- - \nu_{1,n}^{-1}\int_0^{h_1} \psi_{1,n}(y)\phi_x(0, y)\,\mathrm{d}y, \quad n = 0, 1, \ldots, M, \tag{3.4}$$

in which the notation $\nu_{i,n} = k_{i,n}h_i$ has been introduced. It now follows from (3.3) that

$$\phi(0, y_0) = -\sum_{n=0}^{M}(A_n^- + B_n^-)\psi_{1,n}(y_0) + \int_0^{h_1} \sum_{n=M+1}^{\infty} \nu_{1,n}^{-1}\psi_{1,n}(y)\psi_{1,n}(y_0)\phi_x(0, y)\,\mathrm{d}y \tag{3.5}$$

for $0 \leqslant y_0 \leqslant h_1$.

The corresponding construction can be followed through for the domain bounded by $x = \ell$ and $x = \ell + X$. However, it is more direct to transform the variables in (3.3), adjust to the second element of (2.5) and obtain

$$\phi(x_0, y_0) = \sum_{n=0}^{M} A_n^+ \{\exp(k_{1,n}(x_0 - \ell)) + \exp(-k_{1,n}(x_0 - \ell))\}\psi_{1,n}(y_0) - \int_0^{h_1} 2G_1(0, y|x_0 - \ell, y_0)\phi_x(\ell, y)\,\mathrm{d}y,$$

for $\ell \leqslant x_0 \leqslant \ell + X$. The counterparts of (3.4) and (3.5) are respectively

$$B_n^+ = A_n^+ - \nu_{1,n}^{-1} \int_0^{h_1} \psi_{1,n}(y)\phi_x(\ell, y)\,\mathrm{d}y, \quad n = 0, 1, \ldots, M, \tag{3.6}$$

and

$$\phi(\ell, y_0) = \sum_{n=0}^{M} (A_n^+ + B_n^+)\psi_{1,n}(y_0) - \int_0^{h_1} \sum_{n=M+1}^{\infty} \nu_{1,n}^{-1}\psi_{1,n}(y)\psi_{1,n}(y_0)\phi_x(\ell, y)\,\mathrm{d}y \tag{3.7}$$

for $0 \leqslant y_0 \leqslant h_1$.

As the representations (3.5) and (3.7) show, the effect of (2.5) is merely the transfer of modes between the integral terms and the forcing terms.

The derivation of an integral representation of $\phi(x_0, y_0)$ for $0 \leqslant x_0 \leqslant \ell$ makes use of the Green's function

$$G_0(x, y|x_0, y_0) = \sum_{m=-\infty}^{\infty} \{G_2(2m\ell + x, y|x_0, y_0) + G_2(2m\ell - x, y|x_0, y_0)\}$$
$$= \sum_{n=0}^{\infty} \frac{\psi_{2,n}(y)\psi_{2,n}(y_0)}{2\nu_{2,n}\sinh(k_{2,n}\ell)} \{\cosh k_{2,n}(\ell - |x - x_0|) + \cosh k_{2,n}(\ell - x - x_0)\},$$

holding for $(x, y) \neq (x_0, y_0)$ and assuming that $\sin(k_2 h_2) \neq 0$, which satisfies $G_{0x} = 0$ on $x = 0$ and $x = \ell$, $G_{0y} = 0$ on $y = h_2$ and the free-surface condition on $y = 0$. We have introduced the depth

$$h_2 = \max_{0<x<\ell} h(x)$$

to allow for depressions in the bed shape, relative to the level $y = h_1$. If the bedforms under consideration nowhere lie below this level, h_1 can be used in place of h_2 leading to a simpler formulation, but here we seek the maximum generality.

The derivation of an integral form for $\phi(x_0, y_0)$ with $0 \leqslant x_0 \leqslant \ell$ is unaffected by the retention of non-propagating modes outside this interval and is closely based on that given in Porter & Porter (2000). The main feature of the derivation is the use of the Cauchy–Riemann equations to exchange normal and tangential derivatives on $y = h(x)$, a process which introduces the functions

$$\chi_{2,n}(y) = N_{2,n}^{-1/2} \sin k_{2,n}(h_2 - y), \qquad 0 \leqslant y \leqslant h_2, \quad n = 0, 1, 2, \ldots. \tag{3.8}$$

The procedure leads to an integral equation which represents the boundary condition (2.4) applied on $y = h(x)$, namely

$$\int_0^{h_1} m_{21}(x_0, y)q_1(y)\,\mathrm{d}y + \int_0^{\ell} m_{22}(x_0, x)q_2(x)\,\mathrm{d}x + \int_0^{h_1} m_{23}(x_0, y)q_3(y)\,\mathrm{d}y = 0, \quad 0 \leqslant x_0 \leqslant \ell, \tag{3.9}$$

in which we have introduced the functions

$$q_1(y) = \phi_x(0, y), \quad q_3(y) = \phi_x(\ell, y), \quad 0 \leqslant y < h_1,$$
$$q_2(x) = \phi_x(x, h(x)) + h'(x)\phi_y(x, h(x)), \quad 0 < x < \ell.$$

The kernels are given by

$$m_{21}(x_0, y) = \sum_{n=0}^{\infty} \frac{\chi_{2,n}(h(x_0))\psi_{2,n}(y)\sinh k_{2,n}(\ell - x_0)}{\nu_{2,n}\sinh(k_{2,n}\ell)},$$

$$m_{22}(x_0, x) = -\sum_{n=0}^{\infty} \frac{\chi_{2,n}(h(x))\chi_{2,n}(h(x_0))}{2\nu_{2,n}\sinh(k_{2,n}\ell)}\left\{\cosh k_{2,n}(\ell - |x - x_0|) - \cosh k_{2,n}(\ell - x - x_0)\right\}$$

and

$$m_{23}(x_0, y) = \sum_{n=0}^{\infty} \frac{\chi_{2,n}(h(x_0))\psi_{2,n}(y)\sinh(k_{2,n}x_0)}{\nu_{2,n}\sinh(k_{2,n}\ell)}.$$

Integral representations of $\phi(0, y_0)$ and $\phi(\ell, y_0)$ arising from the Green's function formulation in the interval $0 \leqslant x_0 \leqslant \ell$ may be equated with (3.5) and (3.7), respectively, to give the two further equations

$$\int_0^{h_1} m_{11}(y_0, y)q_1(y)\,\mathrm{d}y + \int_0^{\ell} m_{12}(y_0, x)q_2(x)\,\mathrm{d}x + \int_0^{h_1} m_{13}(y_0, y)q_3(y)\,\mathrm{d}y$$
$$= \sum_{n=0}^{M}(A_n^- + B_n^-)\psi_{1,n}(y_0), \quad 0 \leqslant y_0 \leqslant h_1, \quad (3.10)$$

and

$$\int_0^{h_1} m_{31}(y_0, y)q_1(y)\,\mathrm{d}y + \int_0^{\ell} m_{32}(y_0, x)q_2(x)\,\mathrm{d}x + \int_0^{h_1} m_{11}(y_0, y)q_3(y)\,\mathrm{d}y$$
$$= \sum_{n=0}^{M}(A_n^+ + B_n^+)\psi_{1,n}(y_0), \quad 0 \leqslant y_0 \leqslant h_1, \quad (3.11)$$

in which

$$\left.\begin{aligned} m_{11}(y, y_0) &= \sum_{n=M+1}^{\infty} \frac{\psi_{1,n}(y_0)\psi_{1,n}(y)}{\nu_{1,n}} + \sum_{n=0}^{\infty} \frac{\psi_{2,n}(y_0)\psi_{2,n}(y)}{\nu_{2,n}\tanh(k_{2,n}\ell)}, \\ m_{13}(y_0, y) &= -\sum_{n=0}^{\infty} \frac{\psi_{2,n}(y_0)\psi_{2,n}(y)}{\nu_{2,n}\sinh(k_{2,n}\ell)}, \end{aligned}\right\} \quad (3.12)$$

together with

$$m_{12}(y_0, x) = m_{21}(x, y_0), \quad m_{31}(y_0, y) = m_{13}(y, y_0), \quad m_{32}(y_0, x) = m_{23}(x, y_0).$$

We therefore have three coupled integral equations from which to determine q_1, q_2 and q_3, which may be written concisely in the operator form

$$\mathbf{M}\boldsymbol{q} = \sum_{n=0}^{M}\{(A_n^- + B_n^-)\boldsymbol{g}_n^- + (A_n^+ + B_n^+)\boldsymbol{g}_n^+\}, \quad (3.13)$$

holding in the composite Hilbert space $\mathscr{H} = L_2(0, h_1) \oplus L_2(0, \ell) \oplus L_2(0, h_1)$, where

$$\mathbf{M} = \begin{pmatrix} \mathsf{M}_{11} & \mathsf{M}_{12} & \mathsf{M}_{13} \\ \mathsf{M}_{21} & \mathsf{M}_{22} & \mathsf{M}_{23} \\ \mathsf{M}_{31} & \mathsf{M}_{32} & \mathsf{M}_{11} \end{pmatrix}, \qquad \boldsymbol{g}_n^- = \begin{pmatrix} \psi_{1,n} \\ 0 \\ 0 \end{pmatrix}, \qquad \boldsymbol{g}_n^+ = \begin{pmatrix} 0 \\ 0 \\ \psi_{1,n} \end{pmatrix}. \tag{3.14}$$

M_{ij} denotes the operator generated by the real-valued kernel m_{ij} and $\boldsymbol{q} = (q_1, q_2, q_3)^{\mathrm{T}}$.

The space $\mathscr{H}$ is equipped with the inner product

$$[\boldsymbol{q}, \boldsymbol{p}] = (q_1, p_1)_1 + (q_2, p_2)_2 + (q_3, p_3)_1, \tag{3.15}$$

where $\boldsymbol{p} = (p_1, p_2, p_3)^{\mathrm{T}}$ and

$$(q, p)_1 = \int_0^{h_1} q(y)\overline{p(y)}\,\mathrm{d}y, \quad (q, p)_2 = \int_0^{\ell} q(x)\overline{p(x)}\,\mathrm{d}x \tag{3.16}$$

for appropriate p and q.

Thus

$$\boldsymbol{q} = \sum_{n=0}^{M} \{(A_n^- + B_n^-)\boldsymbol{q}_n^- + (A_n^+ + B_n^+)\boldsymbol{q}_n^+\},$$

where $\boldsymbol{q}_n^{\pm}$ satisfy the real integral equation systems

$$\mathbf{M}\boldsymbol{q}_n^{\pm} = \boldsymbol{g}_n^{\pm}. \tag{3.17}$$

Referring to (3.4) and (3.6) we see that

$$B_n^{\pm} = A_n^{\pm} - \nu_{1,n}[\boldsymbol{q}, \boldsymbol{g}_n^{\pm}]$$

and it follows using the notation (2.6) that

$$\boldsymbol{B}^{\pm} = \boldsymbol{A}^{\pm} - \boldsymbol{D}^{-1}\big\{\boldsymbol{Q}^{(-,\pm)}(\boldsymbol{A}^- + \boldsymbol{B}^-) + \boldsymbol{Q}^{(+,\pm)}(\boldsymbol{A}^+ + \boldsymbol{B}^+)\big\},$$

where $\boldsymbol{Q}^{(\pm,\pm)}$ denotes the $(M+1) \times (M+1)$ matrix whose m, n component is $[\boldsymbol{q}_n^{\pm}, \boldsymbol{g}_m^{\pm}]$ (with the plus/minus alternates ordered from left to right) and $D = \mathrm{diag}(\nu_{1,0}, \ldots, \nu_{1,M})$.

We can now identify an expression for the extended scattering matrix defined in (2.7), namely

$$\mathscr{S} = (\mathscr{D} + \mathscr{Q})^{-1}(\mathscr{D} - \mathscr{Q}), \quad \mathscr{D} = \begin{pmatrix} \boldsymbol{D} & 0 \\ 0 & \boldsymbol{D} \end{pmatrix}, \quad \mathscr{Q} = \begin{pmatrix} \boldsymbol{Q}^{(-,-)} & \boldsymbol{Q}^{(+,-)} \\ \boldsymbol{Q}^{(-,+)} & \boldsymbol{Q}^{(+,+)} \end{pmatrix} \tag{3.18}$$

and we find that the extended transfer matrix also introduced in (2.7) is given by

$$\mathscr{P} = \begin{pmatrix} \boldsymbol{Q}^{(+,-)} & \boldsymbol{Q}^{(+,-)} \\ \boldsymbol{D} + \boldsymbol{Q}^{(+,+)} & -\boldsymbol{D} + \boldsymbol{Q}^{(+,+)} \end{pmatrix}^{-1} \begin{pmatrix} -\boldsymbol{D} + \boldsymbol{Q}^{(-,-)} & \boldsymbol{D} + \boldsymbol{Q}^{(-,-)} \\ \boldsymbol{Q}^{(-,+)} & \boldsymbol{Q}^{(-,+)} \end{pmatrix}.$$

Various properties of $\mathscr{S}$ and $\mathscr{P}$ may be deduced from the fact that $\mathsf{M}_{ij}^* = \mathsf{M}_{ji}$, the asterisk denoting the adjoint operator, which implies that $\mathbf{M}$ is a self-adjoint operator on $\mathscr{H}$. Thus $[\mathbf{M}\boldsymbol{p}, \boldsymbol{q}] = [\boldsymbol{p}, \mathbf{M}\boldsymbol{q}]$ for $\boldsymbol{p}, \boldsymbol{q} \in \mathscr{H}$ from which it easily follows that $\mathscr{Q} = \mathscr{Q}^{\mathrm{T}}$. Further, $\overline{\boldsymbol{Q}} = \boldsymbol{Q}$ and $\overline{\boldsymbol{D}} = \boldsymbol{J}\boldsymbol{D}$, where $\boldsymbol{J} = \mathrm{diag}(-1, 1, \ldots, 1)$. Using this information, it can be deduced that $\mathscr{S}$ satisfies the identities

$$\mathscr{S}^{\mathrm{T}} = \mathscr{D}^{-1}\mathscr{S}\mathscr{D}, \quad (\boldsymbol{I} - \mathscr{S})(\boldsymbol{I} + \overline{\mathscr{S}}) = (\boldsymbol{I} + \mathscr{S})\mathscr{J}(\boldsymbol{I} - \overline{\mathscr{S}}), \quad \mathscr{J} = \begin{pmatrix} \boldsymbol{J} & 0 \\ 0 & \boldsymbol{J} \end{pmatrix}, \tag{3.19}$$

where $\boldsymbol{I}$ is the identity matrix, whilst

$$\left.\begin{aligned} \mathscr{P}^{\mathrm{T}} &= \mathscr{E}\mathscr{P}^{-1}\mathscr{E}^{-1}, \qquad \overline{\mathscr{P}} = \mathscr{T}\mathscr{P}\mathscr{T}^{-1}, \\ \mathscr{E} &= \begin{pmatrix} 0 & \boldsymbol{D} \\ -\boldsymbol{D} & 0 \end{pmatrix}, \quad \mathscr{T} = \begin{pmatrix} \frac{1}{2}(\boldsymbol{I}+\boldsymbol{J}) & \frac{1}{2}(\boldsymbol{I}-\boldsymbol{J}) \\ \frac{1}{2}(\boldsymbol{I}-\boldsymbol{J}) & \frac{1}{2}(\boldsymbol{I}+\boldsymbol{J}) \end{pmatrix}. \end{aligned}\right\} \tag{3.20}$$

With $M = 0$, (3.19) reduces to $\mathscr{S}^{\mathrm{T}} = \mathscr{S}$ and $\overline{\mathscr{S}}\mathscr{S} = \boldsymbol{I}$ for the familiar 2×2 scattering matrix, which imply a set of identities between its components first derived by Kriesel (1949). For $M > 0$, (3.19) leads to extensions of the Kreisel relationships which include interactions between between propagating and non-propagating wave modes.

We deduce from the similarity relations (3.20) that the eigenvalues $\lambda_i(K)$ $(i = 0, \ldots, 2M+1)$ of $\mathscr{P}$ must satisfy $\lambda_i\lambda_j = 1$ and $\lambda_i = \overline{\lambda_k}$ for some i, j and k. Therefore the real eigenvalues occur in pairs having reciprocal values and the complex eigenvalues have unit magnitude and occur in conjugate pairs. It follows that we can arrange the spectral representation of $\mathscr{P}$ in the form

$$\mathscr{P} = \mathscr{X}\Lambda\mathscr{X}^{-1} \tag{3.21}$$

where the diagonal matrix Λ of eigenvalues is

$$\Lambda = \begin{pmatrix} \boldsymbol{\Delta} & 0 \\ 0 & \boldsymbol{\Delta}^{-1} \end{pmatrix}.$$

Here $\boldsymbol{\Delta} = \mathrm{diag}(\lambda_0, \ldots, \lambda_M)$ contains those complex eigenvalues of $\mathscr{P}$ with $\arg(\lambda_i) \in (0, \pi)$ followed by the real eigenvalues having magnitude not greater than unity, arranged in order of decreasing magnitude and so that $\boldsymbol{\Delta}^{-1}$ contains the remaining eigenvalues.

In (3.21) we have written $\mathscr{X} = (\boldsymbol{x}_0, \ldots, \boldsymbol{x}_{2M+1})$, where $\boldsymbol{x}_i$ is the eigenvector of $\mathscr{P}$ corresponding to its eigenvalue λ_i. It can be shown using (3.20) that if $\lambda_i\lambda_j \neq 1$ then $\boldsymbol{x}_i^{\mathrm{T}}\mathscr{E}\boldsymbol{x}_j = 0$ and it follows from the way in which the eigenvalues have been partitioned in Λ that

$$\mathscr{X}^{\mathrm{T}}\mathscr{E}\mathscr{X} = \mathscr{E},$$

by an appropriate scaling of the eigenvectors.

The extended transfer matrix $\mathscr{P}_N$ for N contiguous periods of topography is therefore given by

$$\mathscr{P}_N = \mathscr{P}^N = \mathscr{X}\Lambda^N\mathscr{X}^{-1}, \tag{3.22}$$

from which the overall scattering properties represented in (2.12) by $\widehat{\mathscr{S}}_N$ can be determined from (2.9), (2.10) and (2.13) as described in § 2. Care must be taken over the way in which this process is implemented numerically on account of rounding errors associated with the potentially extreme values on the diagonal of the matrix Λ^{-N}. This hazard can be overcome by re-arranging the way in which $\mathscr{S}_N$ is calculated as follows. First we insert (3.22) into the second element of (2.8) and premultiply both sides by $\mathscr{X}^{-1}$. Then the second equation is premultiplied by $\boldsymbol{\Delta}^N$, a step which has the effect of removing all occurrences of the matrix $\boldsymbol{\Delta}^{-N}$. Finally we re-arrange the resulting equations into the form given in the first element of (2.8) leading to

$$\mathscr{S}_N = -\begin{pmatrix} \boldsymbol{X}_{22} & \boldsymbol{\Delta}^N\boldsymbol{X}_{21} \\ \boldsymbol{\Delta}^N\boldsymbol{X}_{12} & \boldsymbol{X}_{11} \end{pmatrix}^{-1} \begin{pmatrix} \boldsymbol{X}_{21} & \boldsymbol{\Delta}^N\boldsymbol{X}_{22} \\ \boldsymbol{\Delta}^N\boldsymbol{X}_{11} & \boldsymbol{X}_{12} \end{pmatrix},$$

where we have written

$$\mathscr{X}^{-1} = \begin{pmatrix} \boldsymbol{X}_{11} & \boldsymbol{X}_{12} \\ \boldsymbol{X}_{21} & \boldsymbol{X}_{22} \end{pmatrix}.$$

The normal scattering matrix $\widehat{\mathscr{S}}_N$ is determined, as before, by means of (2.13).

It may be useful to summarize our approach at this point. No approximation has been made in solving the problem of scattering by a single period of topography. In particular, setting $N = 1$ in (2.13) will give the same conventional scattering matrix $\widehat{\mathscr{S}}_1$, independently of the value of M. We have formulated a sequence of problems for scattering by a single period, indexed by M, the Mth problem being distinguished by the transfer of M evanescent modes from the kernel of the operator M to the right-hand side of (3.13). Thus, all contributions to the full linear specification of the problem have been retained in one location or the other. The purpose of this formulation is to identify, on the basis of computations, the number M of evanescent modes that are required to couple N periods of topography to a given accuracy.

3.2. *Wide-spacing approximation*

An alternative approach is to fix the value of M in advance of carrying out numerical calculations, which has the effect of approximating the overall scattering properties of the ripple bed to an unknown accuracy. From this point of view, the lowest-order approximation is given by setting $M = 0$ throughout the analysis, yielding a formulation commonly referred to as the wide-spacing approximation. In this case, all interactions from evanescent waves between neighbouring periods of topography are neglected. The extended scattering matrix $\mathscr{S}$ then reduces to a 2×2 form which parallels that in (2.12), namely

$$\mathscr{S} = \begin{pmatrix} r^- & -t^+ \mathrm{e}^{\mathrm{i}k_1\ell} \\ -t^- \mathrm{e}^{\mathrm{i}k_1\ell} & r^+ \mathrm{e}^{2\mathrm{i}k_1\ell} \end{pmatrix},$$

where $r^\pm$ and $t^\pm$ are the reflection and transmission coefficients due to waves incident from $x = \pm\infty$ on a single period of topography. We recall that, since $M = 0$, $\widehat{\mathscr{S}}_N = \mathscr{S}_N$ and therefore $\widehat{\mathscr{S}}_1 = \mathscr{S}_1 \equiv \mathscr{S}$ in particular. The corresponding wide-spacing transfer matrix is easily found to be

$$\mathscr{P} = \begin{pmatrix} \mathrm{e}^{\mathrm{i}k_1\ell}(t^- - r^- r^+/t^+) & \mathrm{e}^{\mathrm{i}k_1\ell} r^+/t^+ \\ -\mathrm{e}^{-\mathrm{i}k_1\ell} r^-/t^+ & \mathrm{e}^{-\mathrm{i}k_1\ell}/t^+ \end{pmatrix}.$$

The general theory for the extended transfer matrix applies here and so the two eigenvalues of $\mathscr{P}$ are either complex conjugates, having unit magnitude, or are real and reciprocal, which may easily be confirmed by direct calculation in this special case. Indeed, explicit formulae may be obtained for the eigenvalues and eigenvectors of $\mathscr{P}$ and hence for the components of the overall scattering matrix $\widehat{\mathscr{S}}_N$ defined in (2.12). Related calculations may be found in Evans (1990) and McIver (2001), for example.

Use of the identity $\overline{\mathscr{S}}\mathscr{S} = I$ referred to after (3.20) implies the well-known relationships $t^\pm = |t|\mathrm{e}^{\mathrm{i}\delta}$, $r^\pm = |r|\mathrm{e}^{\mathrm{i}\epsilon_\pm}$, $|r|^2 + |t|^2 = 1$ and $\epsilon_+ + \epsilon_- = 2\delta \pm \pi$. These simplify the determination of $\widehat{\mathscr{S}}_N$ and, in particular, of the expression

$$|T|^2 \equiv |T^\pm|^2 = \frac{|t|^2 \sin^2(\alpha\ell)}{|t|^2 \sin^2(\alpha\ell) + |r|^2 \sin^2(N\alpha\ell)}, \tag{3.23}$$

α being defined by

$$\cos\alpha\ell = \tau \equiv \frac{\cos(\delta + k_1\ell)}{|t|}, \tag{3.24}$$

with $\mathrm{Re}(\alpha\ell) \in [0, \pi]$ and $\mathrm{Im}(\alpha\ell) \geqslant 0$. The eigenvalues of $\mathscr{P}$ are given by $\mathrm{e}^{\pm \mathrm{i}\alpha\ell}$ in this notation. Bragg resonance corresponds to $|\tau| > 1$, for which $\mathrm{Im}(\alpha\ell) > 0$ and therefore $|T^{\pm}| \to 0$ and $|R| \equiv |R^{\pm}| = (1 - |T|^2)^{1/2} \to 1$ as $N \to \infty$. The threshold of resonance is given by $|\tau| = 1$, where $\alpha\ell = 0$ or $\alpha\ell = \pi$.

We note from (3.23) that $|T^{\pm}|$ is bounded below by $|t|^2 \sin^2(\alpha\ell)/\{|t|^2 \sin^2(\alpha\ell) + |r|^2\}$ for all N. This leads to a direct derivation of the envelope R_b the curves of $|R|$ as N varies, in the form

$$|R| \leqslant R_b = \frac{|r|}{|\sin(\delta + k_1\ell)|}, \tag{3.25}$$

a result which has evidently not been given before. This bound applies with $|\tau| \leqslant 1$, which ensures that $R_b \leqslant 1$, and it is such that $R_b = 1$ at $|\tau| = 1$, which is the onset of Bragg resonance.

4. The Bloch problem and sloshing modes

4.1. *The Bloch problem*

We now turn our attention to the extended Bloch problem consisting of (2.15) and (2.17), which we also resolve by integral equation methods.

The most direct approach makes use of the Green's function $G^{\mu}(x, y|x_0, y_0)$ that satisfies

$$\left.\begin{aligned} &\nabla^2 G^{\mu} = -\delta(x - x_0)\delta(y - y_0) \qquad \text{for } 0 < x, x_0 < \ell,\ 0 < y, y_0 < h_2, \\ &G^{\mu}_y + K G^{\mu} = 0 \qquad \text{on } y = 0,\ 0 \leqslant x \leqslant \ell, \\ &G^{\mu}_y = 0 \qquad \text{on } y = h_2,\ 0 \leqslant x \leqslant \ell, \end{aligned}\right\} \tag{4.1}$$

together with the boundary conditions adjoint to (2.17),

$$\left.\begin{aligned} &\mu G^{\mu}(\ell, y|x_0, y_0) = G^{\mu}(0, y|x_0, y_0), \\ &\mu G^{\mu}_x(\ell, y|x_0, y_0) = G^{\mu}_x(0, y|x_0, y_0), \end{aligned}\right\} \quad 0 \leqslant y \leqslant h_2. \tag{4.2}$$

We have again used h_2 to denote the maximum value of $h(x)$ in $0 < x < \ell$.

By expanding G^{μ} in the set of functions $\psi_{2,n}$ or using superposition in the form

$$G^{\mu}(x, y|x_0, y_0) = \sum_{m=-\infty}^{\infty} \mu^m G_2(x - m\ell, y|x_0, y_0),$$

G_2 being given by (3.1), we find that

$$G^{\mu}(x, y|x_0, y_0) = \sum_{n=0}^{\infty} \frac{\psi_{2,n}(y)\psi_{2,n}(y_0)}{2\nu_{2,n}}\, \gamma_n(x - x_0), \qquad (x, y) \neq (x_0, y_0), \tag{4.3}$$

where

$$\gamma_n(x) = \frac{2\mu \sinh(k_{2,n}(\ell - |x|)) + (\mu^2 + 1)\sinh(k_{2,n}|x|) - (\mu^2 - 1)\sinh(k_{2,n}x)}{2\mu\cosh(k_{2,n}\ell) - \mu^2 - 1}, \tag{4.4}$$

provided that $2\mu\cosh(k_{2,n}\ell) \neq \mu^2 + 1$ (a situation that clearly cannot arise in solving the integral equation derived below).

Using (3.2) with $G = G^\mu$ and letting ϕ satisfy the conditions of the Bloch problem leads to the representation

$$-\phi(x_0, y_0) = \int_C \phi(x, y) \frac{\partial}{\partial n} G^\mu(x, y|x_0, y_0)\, \mathrm{d}s, \tag{4.5}$$

for $0 < y_0 < h(x_0)$ and $0 < x_0 < \ell$, where C denotes the bed $y = h(x)$, $0 \leqslant x \leqslant \ell$.

To transform (4.5) into a more convenient form we again employ the technique devised by Porter & Porter (2000) of interchanging normal and tangential derivatives through the Cauchy–Riemann equations. In particular, using $\partial/\partial s$ to denote the derivative along C, we find that

$$\frac{\partial^2 G^\mu}{\partial n \partial n_0} = -\frac{\partial^2 H^\mu}{\partial s \partial s_0},$$

where

$$H^\mu(x, y|x_0, y_0) = \sum_{n=0}^{\infty} \frac{\chi_{2,n}(y)\chi_{2,n}(y_0)}{2\nu_{2,n}} \gamma_n(x - x_0), \qquad (x, y) \neq (x_0, y_0),$$

the functions $\chi_{2,n}$ having been defined in (3.8). We can therefore deduce from (4.5) that

$$-\frac{\partial \phi(x_0, y_0)}{\partial n_0} = \frac{\partial \psi(x_0, y_0)}{\partial s_0} = \frac{\partial}{\partial s_0} \int_0^\ell H^\mu(x, h(x)|x_0, y_0)\, q(x)\, \mathrm{d}x,$$

following an integration by parts, in which

$$q(x) = \phi_x(x, h(x)) + h'(x)\phi_y(x, h(x)), \quad 0 \leqslant x \leqslant \ell,$$

and ψ denotes the stream function. Using the bed condition given in (2.15) and integrating gives

$$\int_0^\ell H^\mu(x, h(x)|x_0, y_0))\, q(x)\, \mathrm{d}x = \psi(x_0, y_0), \quad 0 < y_0 < h(x_0), \quad 0 \leqslant x_0 \leqslant \ell, \tag{4.6}$$

where the constant of integration is found to be zero by setting $\psi(x, h(x)) = 0$ and noting that $H^\mu(x, h(x)|x_0, y_0))$ vanishes at the point on the curve $y_0 = h(x_0)$ where $y_0 = h_2$. Evaluated on $y_0 = h(x_0)$, (4.6) represents a real homogeneous integral equation for the function $q(x)$ expressed by

$$\left.\begin{aligned} (\mathbf{K}^\mu q)(x_0) &\equiv \int_0^\ell k(x, x_0; \mu)\, q(x)\, \mathrm{d}x = 0, \quad 0 \leqslant x_0 \leqslant \ell, \\ k(x, x_0; \mu) &= H^\mu(x, h(x)|x_0, h(x_0)), \quad 0 \leqslant x, x_0 \leqslant \ell, \end{aligned}\right\} \tag{4.7}$$

which may be interpreted as the equation $\mathbf{K}^\mu q = 0$ in $L_2(0, \ell)$.

We therefore seek values $\mu_i(K)$ $(i = 0, 1, \ldots)$ for which (4.7) has non-trivial solutions q_i satisfying $q_i(\ell) = \mu_i q_i(0)$. It should be noted that we have chosen to use $K = \omega^2/g$ rather than k_2, the wavenumber associated with the level h_2, as the parameter in the Bloch problem; this deliberately avoids indicating a preference for any particular depth. The associated Bloch modes can be recovered from (4.6) in the form of their stream functions $\psi_i(x, y)$.

A different approach to the Bloch problem makes use of the formulation given in the previous section, noting that the integral equation (3.9) also applies in the present case. The simplification $q_3(y) = \mu q_1(y)$ for $0 \leqslant y \leqslant h_1$, which follows from

the boundary condition (2.17), and the notational adjustment $q = q_2$ therefore gives

$$\{\mathsf{M}_{21} + \mu\mathsf{M}_{23}\}\, q_1 + \mathsf{M}_{22}\, q = 0 \quad \text{in } L_2(0, \ell), \tag{4.8}$$

using the operator notation of (3.14). A second equation linking q_1 and q arises by taking the limit $M \to \infty$ in (3.10) and (3.11), the resulting infinite sums on the right-hand sides of the equations now representing respectively the expansions of $-\phi(0, y)$ and $\phi(\ell, y)$ in the complete orthogonal set $\psi_{1,n}$ $(n = 0, 1, \ldots)$. Thus

$$\left.\begin{aligned} -\phi(0, y_0) &\equiv \sum_{n=0}^{\infty} (A_n^- + B_n^-)\psi_{1,n}(y_0) = (\widetilde{\mathsf{M}}_{11}q_1 + \mathsf{M}_{12}q + \mu\mathsf{M}_{13}q_1)(y_0), \\ \phi(\ell, y_0) &\equiv \sum_{n=0}^{\infty} (A_n^+ + B_n^+)\psi_{1,n}(y_0) = (\mathsf{M}_{31}q_1 + \mathsf{M}_{32}q + \mu\widetilde{\mathsf{M}}_{11}q_1)(y_0), \end{aligned}\right\} \quad 0 \leqslant y_0 \leqslant h_1, \tag{4.9}$$

where $\widetilde{\mathsf{M}}_{11}$ denotes the operator generated by the kernel $m_{11}(y, y_0)$ given in (3.12) with its first summation term omitted. Use of the boundary condition (2.17) leads directly to

$$\{(1 + \mu^2)\mathsf{M}_{13} + 2\mu\widetilde{\mathsf{M}}_{11}\}\, q_1 + \{\mu\mathsf{M}_{12} + \mathsf{M}_{32}\}\, q = 0 \quad \text{in } L_2(0, h_1). \tag{4.10}$$

The pair of equations (4.8) and (4.10), which may be condensed into the homogeneous matrix operator equation

$$\mathbf{M}^{\mu}\boldsymbol{q} = \mathbf{0} \tag{4.11}$$

holding on the Hilbert space $\mathscr{H}^{\mu} = L_2(0, h_1) \oplus L_2(0, \ell)$, where $\boldsymbol{q} = (q_1(y), q(x))^{\mathrm{T}}$ and

$$\mathbf{M}^{\mu} = \begin{pmatrix} \mathsf{M}_{21} + \mu\mathsf{M}_{23} & \mathsf{M}_{22} \\ (1 + \mu^2)\mathsf{M}_{13} + 2\mu\widetilde{\mathsf{M}}_{11} & \mu\mathsf{M}_{12} + \mathsf{M}_{32} \end{pmatrix}, \tag{4.12}$$

constitutes an alternative version of the extended Bloch problem. It can be confirmed that it reduces to (4.7) on eliminating q_1, a procedure that requires the identities obtained by applying Green's integral formula (3.2) to ϕ, the potential satisfying the conditions of the Bloch problem, and the functions

$$F_n(x, y) = \{\cosh(k_{2,n}x) - \mu\cosh k_{2,n}(\ell - x)\}\psi_{2,n}(y), \quad n = 0, 1, \ldots.$$

Employing the now familiar procedure of transferring between a normal and a tangential derivative in the integral contribution along the bed, we readily arrive at

$$\{1 + \mu^2 - 2\mu\cosh(k_{2,n}\ell)\} \int_0^{h_1} \psi_{2,n}(y)q_1(y)\,\mathrm{d}y = \int_0^{\ell} \{\sinh(k_{2,n}x) + \mu\sinh k_{2,n}(\ell - x)\}\chi_{2,n}(h(x))q(x)\,\mathrm{d}x,$$

for $n = 0, 1, \ldots$.

The advantages of (4.11) over (4.7) are twofold: the eigenvalue parameter μ is not embedded in the kernel and advantage can be taken of computations required by the scattering problem. However, the equation (4.7) remains useful firstly because of its relationship (4.6) to the stream function, which we shall make use of later, and also since it is the more natural formulation to adopt for the computation of sloshing modes where the value of μ is prescribed and the frequency parameter K is

sought. Further, (4.7) offers a straightforward way of examining the eigenvalues of the extended Bloch problem, a step which takes us back to the scattering problem.

4.2. *Relationship to the scattering problem*

We note from (4.7) that the kernel of the operator $\mathbf{K}^{\mu}$ satisfies

$$\overline{k(x, x_0; \mu)} = k(x, x_0; \overline{\mu}) = k(x_0, x; (\overline{\mu})^{-1}),$$

implying that the adjoint of $\mathbf{K}^{\mu}$ satisfies $(\mathbf{K}^{\mu})^* = \mathbf{K}^{(\overline{\mu})^{-1}}$. Hence $\overline{\mu_i(K)}$ is an eigenvalue of the Bloch wave problem with eigenfunction $\overline{q_i}$. Further, using the inner product notation in (3.16), we have

$$(\mathbf{K}^{\mu_i} q_i, q_j)_2 = (q_i, (\mathbf{K}^{\mu_i})^* q_j)_2 = (q_i, \mathbf{K}^{(\overline{\mu_i})^{-1}} q_j)_2 = 0,$$

and therefore $\mu_j = (\overline{\mu_i})^{-1}$ for some i and j. We conclude that the real eigenvalues of the Bloch problem occur in reciprocal pairs and that the complex eigenvalues have unit magnitude and occur in conjugate pairs, properties identical to those of the eigenvalues of the extended scattering matrix. This is not surprising, as (4.7) is equivalent to the coupled equations in (4.11), which are derived from the equations for the scattering case, albeit in the limit $M \to \infty$. To explore the eigenvalue relationship further, we therefore turn again to the development of the scattering case and impose conditions that hold in the Bloch wave problem.

Suppose that ϕ satisfies the extended Bloch boundary conditions (2.17). If these are used in (3.4) and (3.6) and the integral term is eliminated, it follows that $A_n^+ - B_n^+ = \mu(A_n^- - B_n^-)$, for $n = 0, 1, \ldots, M$. Further, substituting (2.17) into (3.5) and (3.7) and using the orthogonality of the functions $\psi_{1,n}$ gives $A_n^+ + B_n^+ = -\mu(A_n^- + B_n^-)$ for $n = 0, 1, \ldots, M$ and

$$\int_0^{h_1} \psi_{1,n}(y)\phi_x(0, y)\,\mathrm{d}y = 0, \quad n = M+1, M+2, \ldots. \tag{4.13}$$

Therefore, $A_n^+ = -\mu B_n^-$ and $B_n^+ = -\mu A_n^-$ for $n = 0, 1, \ldots, M$, and hence, in the notation of (2.6), $(\mathbf{B}^+, \mathbf{A}^+)^{\mathrm{T}} = -\mu(\mathbf{A}^-, \mathbf{B}^-)^{\mathrm{T}}$, which implies in (2.7) that

$$\mathscr{P}\begin{pmatrix} \boldsymbol{A}^- \\ \boldsymbol{B}^- \end{pmatrix} = \mu \begin{pmatrix} \boldsymbol{A}^- \\ \boldsymbol{B}^- \end{pmatrix}.$$

Thus μ is an eigenvalue of $\mathscr{P}$. However, since (4.13) and (3.5) together imply the truncated eigenfunction expansion

$$\phi(0, y) = -\sum_{n=0}^{M} (A_n^- + B_n^-)\psi_{1,n}(y), \tag{4.14}$$

the function ϕ under consideration does not in general satisfy the Bloch problem exactly, but is merely an approximation to a solution. Therefore, μ approximates an eigenvalue of the Bloch problem. We infer that the eigenvalues $\lambda_i(K)$ ($i = 0, 1, \ldots, 2M+1$) of the extended transfer matrix $\mathscr{P}$ are approximations to $2M+2$ of the eigenvalues $\mu_i(K)$ of the extended Bloch problem, the two coinciding as $M \to \infty$.

In particular, the eigenvalues $\mathrm{e}^{\mathrm{i}\beta\ell}$ ($\beta \in \mathbb{R}$) of the usual Bloch wave problem are approximated by the corresponding eigenvalues of $\mathscr{P}$ (if they exist), with increasing accuracy as M increases. The crudest such approximation arises in the wide-spacing case with $M = 0$ and implies that $\alpha \approx \beta$, in the notation of § 3.2, provided that $\alpha \in \mathbb{R}$.

Equation (4.14) provides the corresponding connection between the eigenmode $\phi_i(x, y)$ of the Bloch problem associated with its eigenvalue $\mu_i(K)$ and the eigenvector

$\boldsymbol{x}_i$ of $\mathscr{P}$ belonging to its eigenvalue $\lambda_i(K)$. The two coincide as $M \to \infty$ in the sense that the components of the limiting eigenvector $\boldsymbol{x}_i^{\infty} = (\boldsymbol{A}^-, \boldsymbol{B}^-)^{\mathrm{T}}$ correspond to the coefficients in the exact representation of $\phi_i(0, y)$ in terms of the set $\psi_{1,n}$. To determine components of $\boldsymbol{x}_i^{\infty}$ from the solution of the Bloch problem we may use

$$h_1(A_n^- + B_n^-) = ((\widetilde{\mathsf{M}}_{11} + \mu \mathsf{M}_{13})q_1 + \mathsf{M}_{12}q, \psi_{1,n})_1, \quad n = 0, 1, \ldots,$$

which follows from (4.9) and (3.4), the latter applied in the limit $M \to \infty$ with $\phi_x(0, y)$ replaced by $\phi_{i\,x}(0, y)$.

The relationships derived above allow us, in principle, to use the solution of the Bloch problem to determine the eigenvalues $\lambda_i^{\infty}(K) = \mu_i(K)$ and the eigenvectors $\boldsymbol{x}_i^{\infty}$ of the infinite-dimensional transfer matrix $\mathscr{P}^{\infty}$ which contains information about all of the evanescent modes. In practice, we can determine the eigenvalues and eigenvectors of the truncated form $\mathscr{P}_M^{\infty}$ of $\mathscr{P}^{\infty}$ having the same dimension and structure as the original transfer matrix $\mathscr{P}$. This requires a knowledge of $M + 1$ eigenvalues $\mu_i(K)$ of the Bloch problem, comprising those that are complex and satisfy $\arg(\mu_i) \in [0, \pi]$ together with sufficient real eigenvalues such that $|\mu_i(K)| < 1$, arranged in decreasing order of magnitude. These and the associated eigenvectors, appropriately truncated, allow us to construct the spectral decomposition of $\mathscr{P}_M^{\infty}$ that mimics (3.21).

We may therefore return to the scattering problem and implement a revised approach in which the transfer matrix $\mathscr{P}_M^{\infty}$, derived from the solution of the Bloch problem, is used in place of $\mathscr{P}$. However, we must bear in mind that the scattering problem for a single period has been formulated without approximation. In particular, the spectral properties of $\mathscr{P}$ are exact for each given value of M. Since the sets of eigenvalues $\lambda_i(K)$ and $\mu_i(K)$ coincide in the limit $M \to \infty$, it follows that use of the transfer matrix $\mathscr{P}_M^{\infty}$ to replace $\mathscr{P}$ will only give an accurate solution of the scattering problem if M is sufficiently large.

The relationship between $\lambda_i(K)$ and $\mu_i(K)$ can also be used from the opposite point of view, by inferring the solution of the Bloch problem from that of the scattering problem. Thus, the eigenvalue $\beta(K)$ arising in the usual Bloch wave case is approximated by the corresponding eigenvalue of $\mathscr{P}$, as noted above.

4.3. *The sloshing problem*

As indicated at the end of § 2, in the particular case when there is symmetry in the bedform, expressed as $h(x) = h(\ell - x)$, then certain solutions of the Bloch problem can be used to determine modes of sloshing over a bed containing a finite number of ripples and confined between two vertical walls.

First, we need to restate the Bloch problem in a particular way, which applies only in the case corresponding to the existence of propagating waves over an infinite periodic bed. Rather than aiming to seek values $\mu_i(K)$ as we have set out to do previously in this section, we pose the problem as one in which we seek $K(\beta)$ where $\beta \in \mathbb{R}$ is a given 'propagation constant' such that $\mu = \mathrm{e}^{\mathrm{i}\beta\ell}$ in (4.1) and (4.2). This returns us to the set of equations (2.15) and (2.16), from which the extended Bloch problem was originally conceived, albeit with $K = \omega^2/g$ now playing the role of the eigenvalue parameter.

Consider N periods of topography on the interval $0 \leqslant x \leqslant L = N\ell$ and select the $N + 1$ particular values of β given by

$$\beta = p\pi/N\ell, \quad p = 0, \ldots, N, \tag{4.15}$$

for which we assume we can find values $K(\beta)$ and corresponding eigenfunctions $\phi(x, y)$. With this choice and using (2.16) in (2.14) we observe that

$$\phi(0, y) = (-1)^p \phi(L, y), \quad \phi_x(0, y) = (-1)^p \phi_x(L, y). \tag{4.16}$$

Since the topography is now assumed to be symmetric about $x = \frac{1}{2}\ell$, it is also symmetric about $x = \frac{1}{2}L$ and so we may decompose the potential into its symmetric (ϕ^s) and antisymmetric (ϕ^a) components about this line in the usual manner by writing

$$\phi(x, y) = \phi^s(x, y) + \phi^a(x, y),$$

where

$$\phi^s(x, y) = \phi^s(L - x, y), \quad \phi^a(x, y) = -\phi^a(L - x, y).$$

Using these relations in (4.16) for p even results in the conditions

$$\phi^s_x(0, y) = \phi^s_x(L, y) = 0, \quad \phi^a(0, y) = \phi^a(L, y) = 0,$$

whilst for p odd, we find

$$\phi^s(0, y) = \phi^s(L, y) = 0, \quad \phi^a_x(0, y) = \phi^a_x(L, y) = 0.$$

Although $\phi(x, y)$ is generally a complex-valued eigenfunction the functions ϕ^s and ϕ^a may be chosen to be real without loss of generality by introducing a scaling to $\phi(x, y)$ in such a way that

$$\phi^s(x, y) = \mathrm{Re}\{\phi(x, y)\}, \quad \phi^a(x, y) = \mathrm{Im}\{\phi(x, y)\}. \tag{4.17}$$

Thus, when p is chosen to be even in (4.15), the symmetric potential satisfies Neumann conditions on vertical lines at $x = 0$ and $x = L$. The associated fluid motion represents a free mode of oscillation in a vertically walled tank – a sloshing mode – containing N periods of topography which is symmetric with respect to the centreline of the tank, located at $x = \frac{1}{2}L$. The corresponding antisymmetric potential satisfies Dirichlet conditions on $x = 0$ and $x = L$ and has no such physical interpretation.

When p is odd in (4.15), the antisymmetric potential defined by (4.17) satisfies Neumann conditions on $x = 0$ and $x = L$ and may be intepreted as a sloshing mode in a tank containing N periods of topography which is antisymmetric about $x = \frac{1}{2}L$. Although $\phi^s(x, y)$ satisfies, for p odd, Dirichlet conditions on $x = 0$ and $x = L$, it does satisfy a Neumann condition on $x = \frac{1}{2}L$, which may therefore be replaced by a vertical wall. A physical interpretation of flow described by this potential follows from the antisymmetric reflection of the potential across either of the boundaries $x = 0$ and $x = L$, again resulting in a sloshing mode in a vertically walled tank containing N periods which is antisymmetric about its centreline.

Streamline patterns for the four types of modes described above can be identified in figure 1 in the case of $N = 2$. These results will be discussed in detail in § 5.

The appropriate form of the Green's function for determining sloshing modes is given by (4.3), with the substitution $\mu = \mathrm{e}^{\mathrm{i}\beta\ell}$ into (4.4) resulting in

$$\gamma_n(x) = \frac{\sinh k_{2,n}(\ell - |x|) + \cos\beta\ell \sinh k_{2,n}|x| + \mathrm{i}\sin\beta\ell \sinh k_{2,n}x}{\cosh k_{2,n}\ell - \cos\beta\ell}.$$

Two special cases arise where the generally complex Green's function reduces to a real function: for $\beta = 0$, with

$$\gamma_n(x) = \frac{\cosh k_{2,n}\left(\frac{1}{2}\ell - |x|\right)}{\sinh \frac{1}{2}k_{2,n}\ell};$$

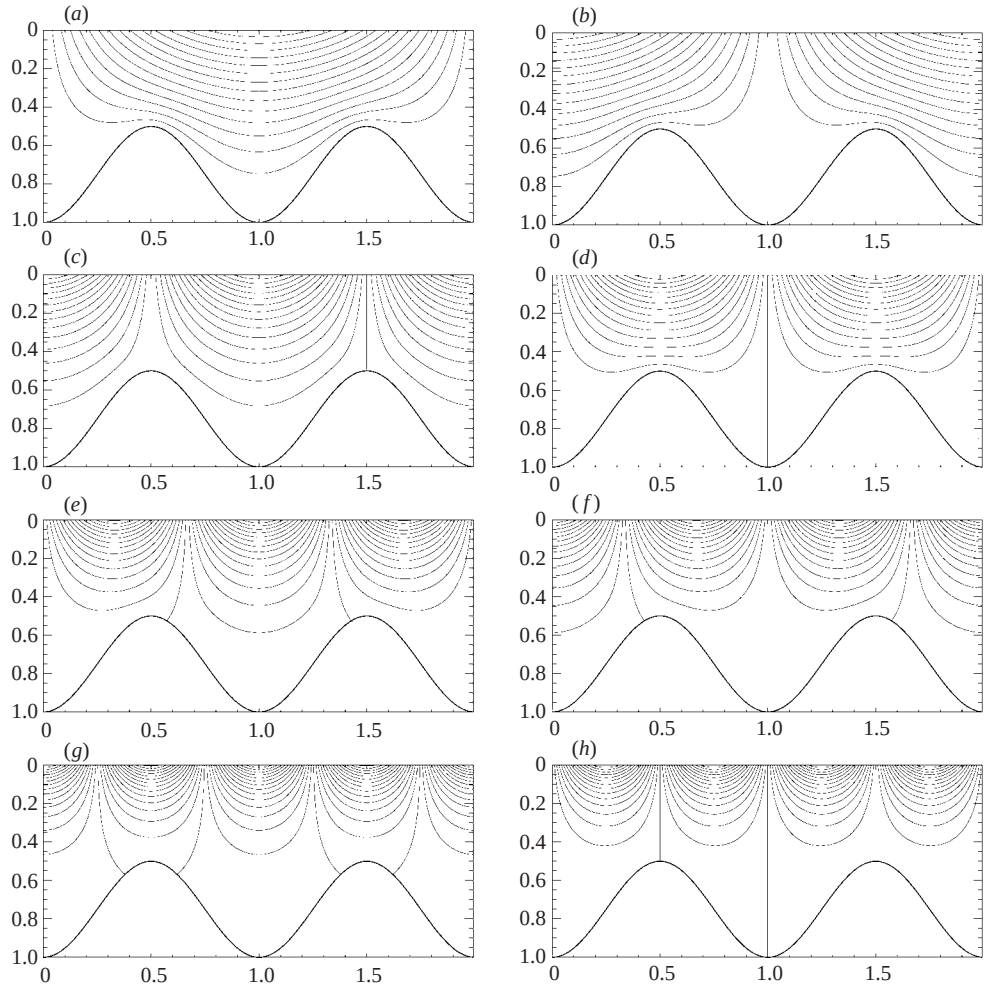

FIGURE 1. Streamlines of the sloshing modes for $N = 2$ periods of symmetric topography in a vertical-walled tank, $\ell/h_2 = 1$: (a, c, e, g) on the left correspond to ϕ^a, and (b, d, f, h) on the right correspond to ϕ^s. (a, b) Generated using $p = 1$ ($\beta\ell = \frac{1}{2}\pi$) occurring at $K\ell = 1.1720$; (c, d) using $p = 2$ ($\beta\ell = \pi$) occurring at $K\ell = 2.9508$ for (c) and $K\ell = 3.0739$ for (d); (e, f) using $p = 1$ ($\beta\ell = \frac{1}{2}\pi$) occurring at $K\ell = 4.6847$; and (g, h) using $p = 0$ ($\beta\ell = 0$) occurring at $K\ell = 6.2771$ for (g) and $K\ell = 6.2780$ for (h).

and for $\beta\ell = \pi$, with

$$\gamma_n(x) = \frac{\sinh k_{2,n}\left(\frac{1}{2}\ell - |x|\right)}{\cosh \frac{1}{2}k_{2,n}\ell}.$$

The two associated Green's functions apply to sloshing modes over a single period of symmetric topography between vertical walls.

When the bedform $h(x)$ has no symmetry, it is expected that sloshing modes also exist for those values of β given by (4.15), but contained between non-vertical walls (see, for example, Porter & Evans 1999).

5. Results

5.1. *Method of solution*

In this paper we have considered three different types of problem all involving the interaction of waves with a single period of topography, for scattering, Bloch waves and sloshing modes. In each case we have formulated the problem in terms of integral equations. We shall describe the method of solution for the most complicated situation of scattering, in which there are three coupled equations, indicating how this can adapted to the simpler Bloch and sloshing problems.

The scattering problem to be solved is similar to that described in Porter & Porter (2000) for waves propagating over a bed with a depression, with the simplification that the depths of the fluid on the right and left of the varying topography are equal in the present case. However, instead of the single unknown vector occurring in the earlier work, here we must calculate the further vectors that arise from evanescent waves being cast in the role of forcing terms. These additional free terms add little to the computational cost, the bulk of the effort being devoted to evaluating the kernels of the integral operators and as this aspect was fully discussed in Porter & Porter (2000), it is not repeated here in detail.

The solutions $\boldsymbol{q}_n^{\pm}$ of the integral equations in (3.17) are approximated by writing

$$\boldsymbol{q}_n^{\pm} \simeq \tilde{\boldsymbol{q}}_n^{\pm} = \sum_{s=0}^{S} c_{n,s}^{\pm} \boldsymbol{p}_s, \quad n = 0, \ldots, M, \tag{5.1}$$

where $c_{n,s}^{\pm}$, $s = 0, \ldots, S$, are coefficients to be determined. Here, $S = S_1 + S_2 + S_3 + 2$ involves three independent truncation parameters and $\boldsymbol{p}_n = (u_n(y), 0, 0)^{\mathrm{T}}$ for $n = 0, \ldots, S_1$, $\boldsymbol{p}_{n+S_1+1} = (0, v_n(x), 0)^{\mathrm{T}}$ for $n = 0, \ldots, S_2$ and $\boldsymbol{p}_{n+S_1+S_2+2} = (0, 0, w_n(y))^{\mathrm{T}}$ for $n = 0, \ldots, S_3$. The choice of the sets of functions $\{u_n(y)\}, \{v_n(x)\}, \{w_n(y)\}$ that are best suited to the particular problem under consideration is described in detail in Porter & Porter (2000) and is related to the way the varying bed joins the level depths at $x = 0$ and $x = \ell$. For smoothly joining bed shapes, the choice

$$u_n(y) = w_n(y) = h_1^{-1} \psi_{1,n}(y), \quad 0 \leqslant y \leqslant h_1, \tag{5.2a}$$

for $n = 0, \ldots, S_1$ with $S_1 = S_3$ and

$$v_n(x) = \ell^{-1} \cos(n\pi x/\ell), \quad 0 \leqslant x \leqslant \ell, \tag{5.2b}$$

for $n = 0, \ldots, S_2$ is appropriate. Although rapid convergence of results can be achieved for non-smooth bed joins at $x = 0$ and $x = \ell$ by using the more exotic choice of functions described in Porter & Porter (2000), those prescribed above are more than adequate for the present purposes.

Substituting the approximation (5.1) into the integral equations and taking the inner product as defined by (3.15) with $\boldsymbol{p}_m$ gives the system of algebraic equations

$$\sum_{s=0}^{S} c_{n,s}^{\pm} [\mathbf{M} \boldsymbol{p}_s, \boldsymbol{p}_m] = [\boldsymbol{g}_n^{\pm}, \boldsymbol{p}_m], \quad m = 0, \ldots, S, \tag{5.3}$$

for $n = 0, \ldots, M$. Porter & Porter (2000) showed that this solution process, which is an application of Galerkin's method, is equivalent to a variational formulation. It

follows that the quantities of prime interest, the elements

$$\mathscr{Q}^{(\pm,\pm)}_{m,n} = [\boldsymbol{q}^{\pm}_n, \boldsymbol{g}^{\pm}_m] \simeq \sum_{s=0}^{S} c^{\pm}_{n,s} [\boldsymbol{p}_s, \boldsymbol{g}^{\pm}_m], \tag{5.4}$$

of the blocks forming the matrix $\mathscr{Q}$ given in (3.18), are obtained to second-order accuracy. As previously, the plus/minus alternates are ordered from left to right in the equation above. We note that the matrix of elements $[\mathbf{M}\boldsymbol{p}_s, \boldsymbol{p}_m]$ in (5.3) is real and symmetric and that the right-hand side terms $[\boldsymbol{g}^{\pm}_n, \boldsymbol{p}_m]$ are also real.

We refer the reader to Porter & Porter (2000) for a detailed description of how to perform the numerical computation of the solutions to (5.3) and (5.4).

The pair of coupled equations that constitute (4.11) for the extended Bloch problem can be dealt with the same general way, leading to a system of homogeneous algebraic equations involving the parameter μ. We write

$$\boldsymbol{q} \simeq \tilde{\boldsymbol{q}} = \sum_{s=0}^{S} c_s \boldsymbol{p}_s, \quad n = 0, \ldots, M,$$

with adjusted definitions of $S = S_1 + S_2 + 1$ and $\boldsymbol{p}_n = (u_n(y), 0)^{\mathrm{T}}$, for $n = 0, \ldots, S_1$, $\boldsymbol{p}_{n+S_1+1} = (0, v_n(x))^{\mathrm{T}}$, for $n = 0, \ldots, S_2$. Application of Galerkin's method in this case results in the system of equations given by

$$\sum_{s=0}^{S} c_s \langle \mathbf{M}^{\mu} \boldsymbol{p}_s, \boldsymbol{p}_m \rangle = \mathbf{0}, \qquad m = 0, \ldots, S, \tag{5.5}$$

where $\langle \boldsymbol{q}, \boldsymbol{p} \rangle = (q_1, p_1)_1 + (q_2, p_2)_2$, in the notation of (3.16), is the inner product on the space $\mathscr{H}^{\mu}$ and $\mathbf{M}^{\mu}$ is given by (4.12). Solutions of the extended Bloch problem are approximated by the non-trivial solutions of (5.5).

The approach outlined above for the numerical determination of the eigenvalues, $\mu_i(K)$, of the extended Bloch problem is particularly useful since the eigenvalue parameter μ appears explicitly in (4.12) and hence in its approximation (5.5). The merit of this feature will be discussed in further detail in § 5.4.

The method for approximating the solution of the scalar integral equation (4.7) for the Bloch problem and the corresponding equations for sloshing is also very similar, albeit much simpler and more transparent. In both the Bloch and sloshing cases we write

$$q(x) \simeq \tilde{q}(x) = \sum_{s=0}^{S} c_s v_s(x) \tag{5.6}$$

for unknown coefficients c_s, $s = 0, \ldots, S$, where the set $\{v_n(x)\}$ is defined in (5.2) and $S = S_2$. Substituting the approximation (5.6) into (4.7) and taking the inner product $(.,.)_2$, defined in (3.16), with the function $v_m(x)$, results in the homogeneous system of equations

$$\sum_{s=0}^{S} c_s (\mathbf{K}^{\mu} v_s, v_m)_2 = 0, \qquad m = 0, \ldots, S. \tag{5.7}$$

The non-trivial solutions of this system of equations determine the approximations to the Bloch modes (by fixing the frequency parameter K and determining values of μ) or the sloshing modes (by fixing $\beta \in [0, \pi]$ where $\mu = \mathrm{e}^{\mathrm{i}\beta\ell}$ and determining the frequency parameter K).

We note that with $\mu = e^{i\beta\ell}$ and $\beta \in \mathbb{R}$, the integral operator $\mathbf{K}^\mu$ is self-adjoint and therefore its eigenvalues are real. This property is inherited by the system (5.7) so that the eigenvalues of the matrix having elements $(\mathbf{K}^\mu v_s, v_m)_2$, which approximate the eigenvalues of $\mathbf{K}^\mu$, are also real.

5.2. *Numerical procedure*

Numerical results obtained for the scattering problem have been verified using a number of independent checks of accuracy. The method of Porter & Porter (2000) can only produce efficient and accurate computational results for relatively short bed lengths and soon becomes unwieldy as N increases. However, using that method for a number of cases in which the N periods of topography are regarded as a single continuous bedform confirms that the calculations based on extended transfer matrices do indeed converge to the correct results as M, the number of evanescent terms retained in the exchange of information between adjacent periods, increases. There also exists a substantially simplified version of the extended transfer matrix formulation in the case for which the periodic topography is entirely elevated above the level $y = h_1$, because only one Green's function is required. This special case has not been presented here, but it has been used to provide an independent check of the numerical implementation of our more general formulation, for the bedforms that conform to $h_2 = h_1$.

There are a number of stages in the numerical calculation that require approximation or truncation, some of which have already been introduced explicitly. We shall now briefly indicate where these approximations arise and what schemes have been implemented in the computations, as a result of extensive numerical experiments; our goal is to produce results that are accurate to at least four decimal places. Although this aim exceeds all realistic practical purposes, we have set out to produce results that are 'exact', within the scope of linear theory, primarily to show that this can be achieved with relative efficiency but also to provide a means by which the performance of approximate theories, such as those based on the mild-slope equations, can be assessed.

First, there are several infinite sums that need to be computed that are associated with the definition of the matrix of kernels, m_{ij}, $i, j = 1, 2, 3$, of integral operators. In most cases, series resulting from the implementation of the approximation to the integral equations converge like $1/n^2$ and in these cases the infinite sums are truncated at the 4000th term. In some cases, the series converge exponentially and are truncated when eight-figure accuracy has been attained. One of the series in particular, associated with the kernel $m_{22}(x, x_0)$, is logarithmically singular. This singularity is removed and integrated out explicitly (see Porter & Porter 2000) to leave a series which converges like $1/n^2$. Secondly, whilst some integration can be performed analytically, quadrature must be used for integrands that involve the arbitrary bed function, $h(x)$. A composite ten-point Gaussian quadrature is employed for this purpose involving 200 evaluations of the integrand per integral. Numerical experimentation suggests that this scheme produces approximations to integrals that are accurate to seven significant figures.

Next, we need to adopt values for the truncation parameters S and M which, respectively, represent the number of terms used in the approximation to the solution of the integral equations and the number of evanescent terms that are incorporated into the extended transfer matrix. We have already inferred that results become increasingly accurate as both S and M are increased but for computational purposes wish to keep M and, in particular, S as small as possible. In fact, it turns out that

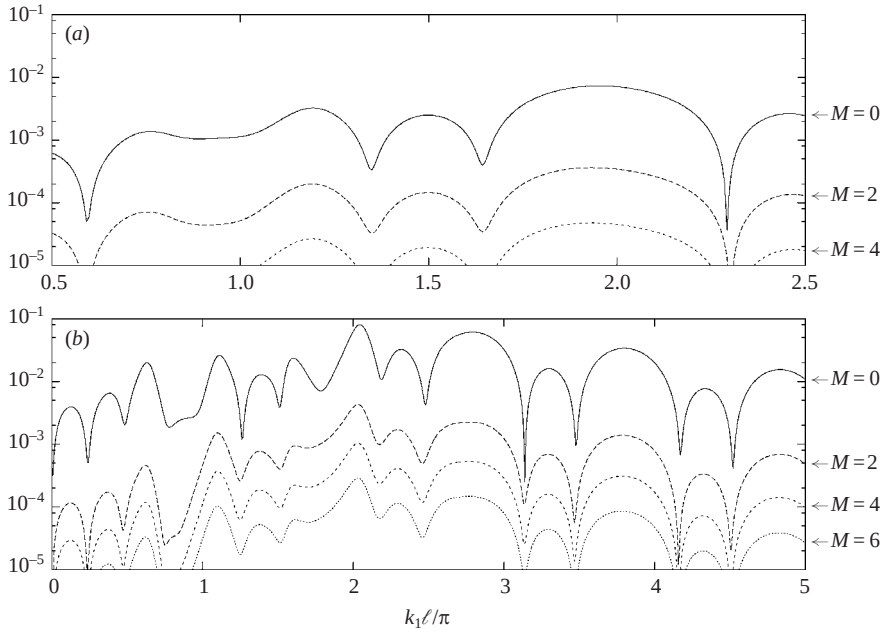

FIGURE 2. Convergence of $|R|$ with M corresponding to (a) figure 4 and (b) figure 6. Vertical scale measures $|R - R_e|$ where R_e uses $M = 10$ and R uses $M = 0, 2, 4, 6$.

only relatively small values are needed. Numerical experiments suggest that $M = 4$ is sufficient for the desired overall accuracy, in most cases. The essential criterion for the choice of S is that its component truncation parameters, $S_1 = S_3$ and S_2, must be large enough to accurately model the functions $q_1(y)$, $q_3(y)$ over the depth $0 < y < h_1$ and $q_2(x)$ over the bed $h(x)$ for $0 \leqslant x \leqslant \ell$. In particular, if either $h(x)$ is rapidly varying or the wave frequency is high (or both) then more functions will be required in the expansion of $q(x)$, relating to the tangential fluid velocity on the bed. In most circumstances a value of $S_2 = 12$ is sufficient. In the most extreme case encountered in the present paper, of the doubly periodic bed defined by (5.9) with $k\ell$ large (see figure 6), values of $M = 8$ and $S_2 = 24$ were used to ensure four-decimal-place accuracy in $|R|$ and $|T|$. On the other hand relatively few functions are needed to model the structure of the horizontal fluid velocity across the vertical lines $x = 0$ and $x = \ell$, represented by the functions $q_1(y)$ and $q_3(y)$. For the series representing these velocities, a truncation level of $S_1 = S_3 = 8$ was found to be sufficient for the required accuracy in all cases.

The convergence of the numerical method with increasing values of M is illustrated in figures 2(a) and 2(b) corresponding to the curves of $|R|$ shown in figures 4 and 6, the severe case mentioned previously. In figure 2 we compare successive estimates of R using $M = 0, 2, 4, 6$ with a value R_e, computed using $M = 10$, by plotting the error $|R - R_e|$ over a range of values of $k_1\ell/\pi$. It can be seen that with $M = 0$, corresponding to the wide-spacing approximation, the error can approach 0.1, representing a relative error of nearly 10%. As expected, the convergence displayed in figure 2(a) is faster than that in figure 2(b), for a steeper and more complicated bedform. Convergence for topographies with continuous derivatives at $x = 0$ and $x = \ell$, such as those described by (5.10) is even better than that in the cases presented here. Notice that the error peaks at values around $k_1\ell = 2\pi$. As $k_1\ell \to \infty$ (high frequency), we would expect the

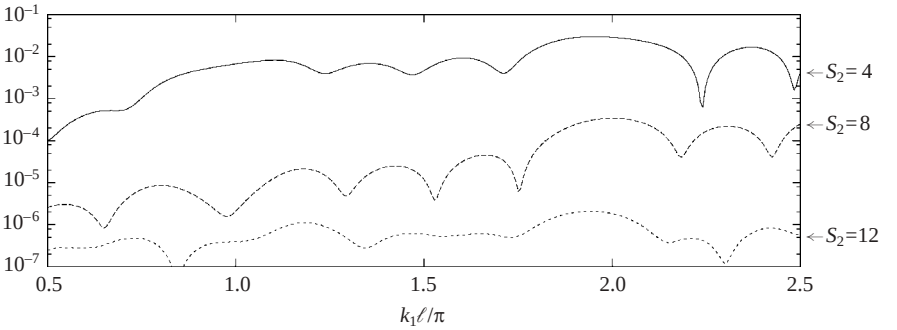

FIGURE 3. Convergence of $|R|$ with truncation parameter S_2 corresponding to figure 4. Vertical scale measures $|R - R_e|$ where R_e uses $S_2 = 24$ and R uses $S_2 = 4, 8, 12$.

wide-spacing approximation to become increasingly good and this is confirmed by our results.

Figure 3 illustrates the convergence of the numerical scheme with truncation parameter S_2 in a typical case, corresponding to the curve in figure 4. Again $|R - R_e|$ measures the error in R for increasing values of S_2 compared with R_e computed using $S_2 = 24$ and with a fixed value of $S_1 = 12$. In this case $S_2 = 12$ produces results accurate to nearly six figures for the range of $k_1\ell$ considered.

5.3. *Results for the scattering problem*

The sinusoidal bed used by Davies & Heathershaw (1984) is given by (2.1) with

$$h(x) = h_1 - b\sin(2\pi x/\ell). \tag{5.8}$$

The doubly periodic bed used by Guazelli *et al.* (1992) and later Chamberlain & Porter (1995*a*) is

$$h(x) = h_1 - \tfrac{1}{2}b[\sin(2\pi x/\ell) + \sin(4\pi x/\ell)], \tag{5.9}$$

where the amplitude of the bed fluctuations satisfies $|h(x) - h_1| < 0.877b$. The other bedforms used in this paper is are given by

$$h(x) = h_1 \pm \tfrac{1}{2}b[1 - \cos(2\pi x/\ell)], \tag{5.10}$$

which represents wholly elevated (plus sign) and wholly depressed (minus sign) periodic topography.

The results in the figures 4–6 have been chosen to allow comparison with a set of curves presented in Chamberlain & Porter (1995*a*). Those authors were comparing the performance of their so-called modified mild-slope equation (MMSE) with the mild-slope equation (MSE) originally due to Berkhoff (1973) and the extended mild-slope equation derived by Kirby (1986) specifically to allow for scattering by ripple beds. The MSE and MMSE are approximations to full linear theory and are based on the assumption that the bed slope is small in the sense that $|kh'/h| \ll 1$. Chamberlain & Porter (1995*a*) were especially interested in periodic bed topography for which the MSE gives values of $|R|$ which are markedly out of line with the experimental results of Davies & Heathershaw (1984) near Bragg resonance. In the cases considered by Chamberlain & Porter (1995*a*), comparison is also possible with results of Guazzelli *et al.* (1992) and the computations of O'Hare & Davies (1993). We have computed reflection coefficients that correspond to these cases using the method presented in this paper. In each of figures 4–6 we have also included results computed using the

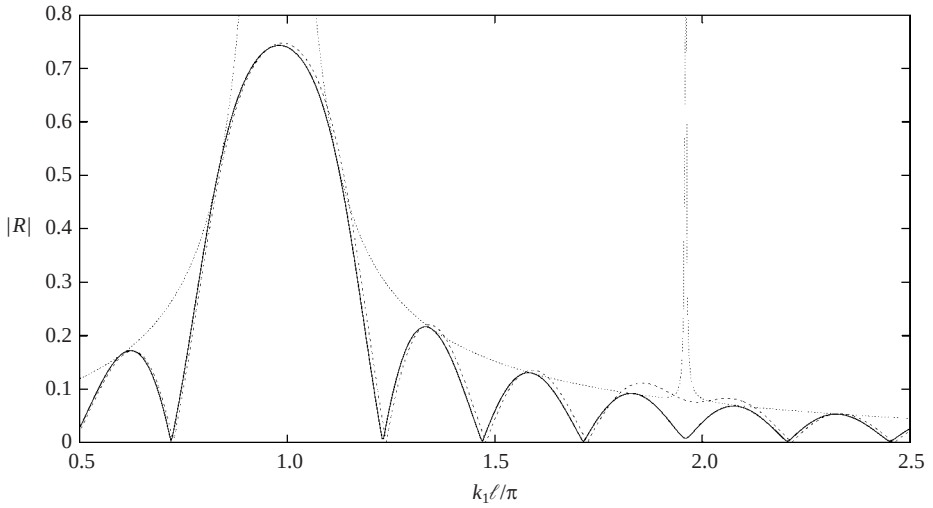

FIGURE 4. Variation of $|R|$ (solid curve) with non-dimensional frequency parameter $k_1\ell/\pi$ for $N = 4$ periods of sinusoidal topography with $b/h_1 = 0.32$, $\ell/h_1 = 6.4$. The dashed curve is results obtained from the modified mild-slope equations. The dotted curve is the $M = 0$ (wide spacing) bound on $|R|$.

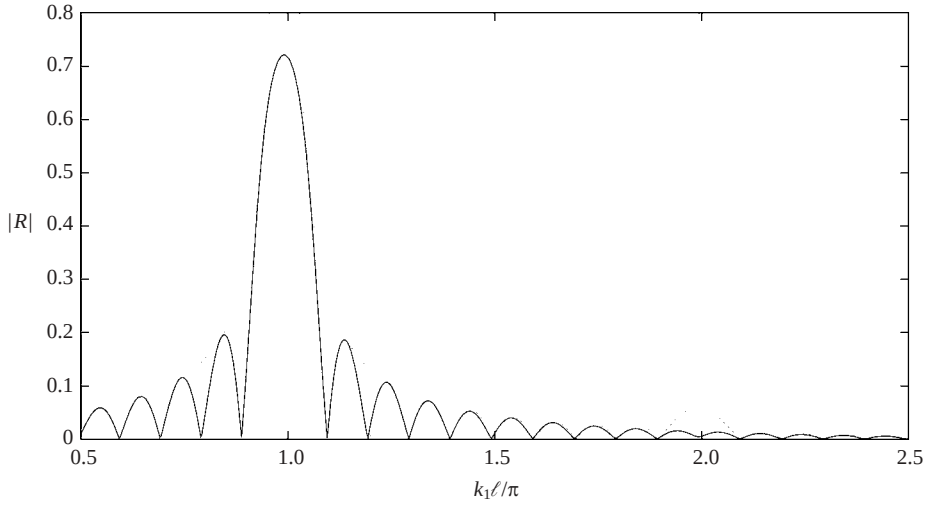

FIGURE 5. Variation of $|R|$ (solid curve) with non-dimensional frequency parameter $k_1\ell/\pi$ for $N = 10$ periods of sinusoidal topography with $b/h_1 = 0.16$, $\ell/h_1 = 3.2$. The dashed curve is results obtained from the modified mild-slope equations. The dotted curve is the $M = 0$ (wide spacing) bound on $|R|$.

MMSE. In figures 4 and 5, where the topography is such that the bed slope is small, the MMSE compares very favourably with the exact results apart from, in both cases, values close to $k_1\ell = 2\pi$ where the MMSE exaggerates the second-order Bragg resonance. The sinusoidal topography defined by (5.8) was used in figures 4 and 5 with parameters given in the figure captions. The correspondence between the present

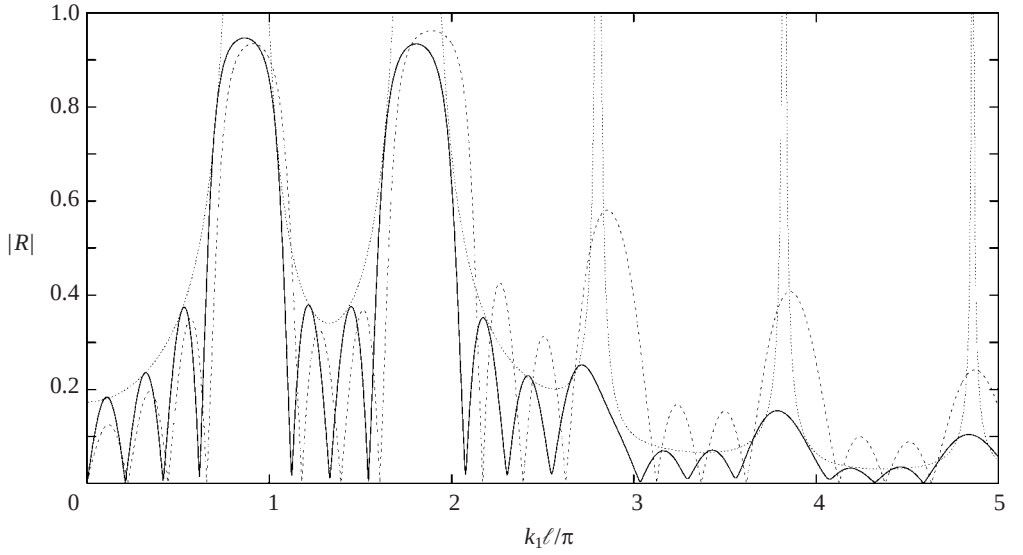

FIGURE 6. Variation of $|R|$ (solid curve) with non-dimensional frequency parameter $k_1\ell/\pi$ for $N = 4$ periods of doubly sinusoidal topography with $b/h_1 = 0.8$, $\ell/h_1 = 4.8$. The dashed curve is results obtained from the modified mild-slope equations. The dotted curve is the $M = 0$ (wide spacing) bound on $|R|$.

full linear calculations and the results given by the MMSE confirm that the extra terms proportional to $h'(x)$ and $h''(x)$ included in that equation and not in the MSE can be important.

The success of the MMSE in approximating reflection coefficients for periodic topography is limited, however, as the results in figure 6 reveal. In that figure, the doubly periodic sinusoidal topography defined by (5.9) is considered with parameters given in the figure caption. The combined effect of the extra complexity of the bed shape and the steeper bed slope appears to significantly affect the accuracy of the results based on MSE models, and this is not surprising.

An interesting feature of the results presented in figure 6 is the non-zero values that $|R|$ takes at the bottom of the 'cusps' (for example near $k_1\ell/\pi \approx 2.5$). A detailed numerical study near these points has revealed that the curves of $|R|$ actually have smooth, non-zero local minima there. This is in contrast to the approximate results obtained from using wide spacing (i.e. $M = 0$) in which it is easy to confirm from the expression given for $|T|$ in (3.23) that zeros of reflection occur at these locations. Similarly, the MSE and its variants give zeros of $|R|$ at such points (see, for example, Chamberlain & Porter 1995*b*). Further detailed investigation of the local minima in the results computed in figure 6 show that there appears to be a periodic structure in the values of $|R|$ at these local minima with absolute zeros being obtained when $k_1\ell/\pi$ approximately equals $\pi/2$, π, $3\pi/2$.

Figures 4–6 also include a curve of R_b given by (3.25), which is the simple expression for the upper bound on $|R|$ based on the wide-spacing ($M = 0$) approximation. In all three cases these curves are very close to being upper bounds for the values of $|R|$ determined with $M \geqslant 1$, which are accurate to at least four decimal places. This may seem surprising given, for example, the size of the error in R for $M = 0$ shown in figure 2 corresponding to the curves in figure 6. It is due to the fact that the

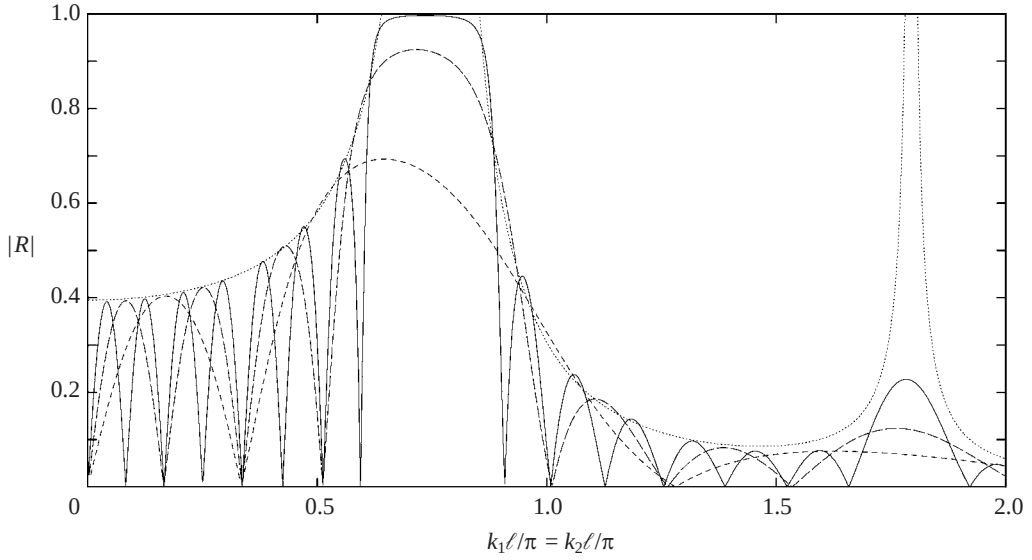

FIGURE 7. Variation of $|R|$ with non-dimensional frequency parameter $k_1\ell/\pi$ for a $N = 2$ (short dash), $N = 4$ (long dash) and $N = 8$ (solid) periods of elevated cosine topography with $b/h_1 = \frac{3}{4}$, $\ell/h_1 = 2$. The dotted curve is the $M = 0$ (wide spacing) bound on $|R|$.

wide-spacing approximation predicts quite accurately the height of the peaks in $|R|$ apart from that in the neighbourhood of Bragg resonance ($k_1\ell \approx n\pi$), where $R_b = 1$. The other source of error in the wide-spacing approximation is due to a translation of the peaks of $|R|$.

In the final two figures illustrating Bragg resonance in scattering problems, we consider two related topographies and investigate the effect of changes in N, the number of periods. Figure 7 shows the variation of $|R|$ for $N = 2, 4, 8$ in the case of sinusoidal topography defined by (5.10) and entirely elevated above the level h_1 so that $h_2 = h_1$, $\ell/h_2 = 2$ and $b/h_2 = \frac{3}{4}$. The results in figure 8 are also for $\ell/h_2 = 2$ and $b/h_2 = \frac{3}{4}$, but here the topography is entirely depressed below the level h_1. Thus the two examples differ only in the way the topography joins the levels in $x < 0$ and $x > N\ell$. To assist in the comparison between figures 7 and 8, $|R|$ is measured in both cases against the wavenumber $k_2\ell/\pi$, local to the periodic topography.

Figures 7 and 8 are clearly very similar. In both cases, the curve of R_b has been included and again serves well as an approximate envelope to the values of $|R|$ for different values of N. It is noticeable – especially at second-order Bragg resonance near $k_2\ell = 2\pi$ – that the curve of R_b provides a much better approximation to the peaks of $|R|$ in figure 8 than in figure 7. This is easily explained by the fact that waves interacting with depressed topography will inevitably generate smaller contributions to outgoing evanescent modes than elevated topography. However, it is particularly surprising that the curves of R_b in figures 7 and 8 intersect the line $|R| = 1$ at approximately the same four points, even though the curve of R_b is generated using the transmission coefficient for a single period of topography ($N = 1$) and those arising in the two figures are therefore generated by quite different problems. To understand why this is so, and to explain other aspects of the results in figures 7 and 8, we turn to the results of the Bloch problem.

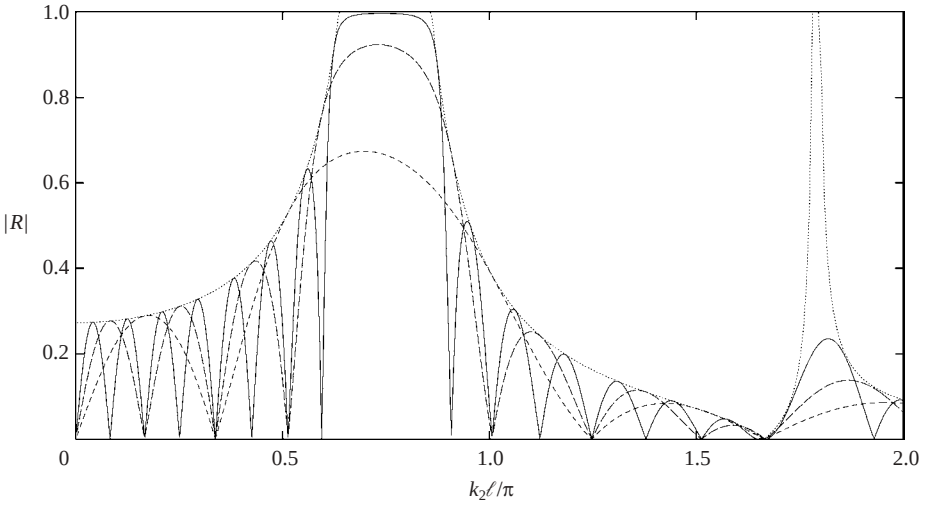

FIGURE 8. Variation of $|R|$ with non-dimensional frequency parameter $k_2\ell/\pi$ for a $N = 2$ (short dash), $N = 4$ (long dash) and $N = 8$ (solid) periods of depressed cosine topography with $b/h_2 = \frac{3}{4}$, $\ell/h_2 = 2$. The dotted curve is the $M = 0$ (wide spacing) bound on $|R|$.

5.4. *Results for the Bloch and sloshing problems*

In § 4 it was proved that the eigenvalues of the Bloch problem satisfy either $\mu_i(K) \in \mathbb{R}$ or $\mu_i(K) = \mathrm{e}^{\mathrm{i}\beta\ell}$ where $\beta \in \mathbb{R}$. The Bloch problem involves fixing the frequency parameter K and solving for a set, μ_i, $i = 0, \ldots, M$, of eigenvalues. On account of the reciprocity relations between eigenvalues of the Bloch problem referred to in § 4, only those eigenvalues with $\arg(\mu_i) \in [0, \pi]$ and $|\mu_i| \leqslant 1$, $i = 0, \ldots$, need to be found, the remaining eigenvalues being given by $1/\mu_i$, $i = 0, \ldots$.

Solutions of the Bloch problem are given by the non-trivial solutions of (4.7) which reduces by Galerkin's method to finding the non-trivial solution of the system of equations (5.7). Alternatively, we may use the approximations made to the pair of coupled integral equations in (4.11) using Galerkin's method to reduce its solution to (5.5) and this latter approach has advantages. First, use can be made of the related calculations that are required in the solution of the scattering problem due to the elements common to the two formulations. More importantly from a numerical perspective, is that the eigenvalue parameter, μ, is not embedded in the kernel of the various integral operators and only appears algebraically in the definition of $\mathbf{M}^{\mu}$ in (4.12). Thus, for each value of the frequency parameter K, only one set of matrix elements needs to be computed and then, in principle, the set $\mu_i(K)$, $i = 0, 1, 2, \ldots$ of eigenvalues can all be found extremely efficiently using a standard numerical root-finding routine. In practice, it is only useful for locating those eigenvalues $\mu_i(K)$ which are real since then the problem is equivalent to locating zeros of a real determinant. On the other hand, when $\mu = \mathrm{e}^{\mathrm{i}\beta\ell}$, the matrix in (5.5) derived from the approximation to (4.11) is not automatically Hermitian by construction and small rounding errors in the calculation of the various matrix elements make the determination of zeros of a now complex determinant much more difficult. Thus, for the complex eigenvalues it is much more straightforward to implement the approximation to the scalar integral equation (4.7). This approach has the disadvantage that the eigenvalue parameter is embedded in the kernel of the integral operator. However, the approximation of (4.7)

Scattering:	$\arg(\lambda_0)$	$\lambda_1 \times 10^2$	$\lambda_2 \times 10^4$	$\lambda_3 \times 10^6$	$\lambda_4 \times 10^8$
$M = 0$	1.73112	–	–	–	–
$M = 1$	1.72830	0.77453	–	–	–
$M = 2$	1.72781	0.95100	0.21621	–	–
$M = 3$	1.72781	0.95224	0.42772	0.3989	–
$M = 4$	1.72781	0.95225	0.44779	0.1900	6.24
$M = 5$	1.72781	0.95227	0.44801	0.2395	0.39
$M = 6$	1.72781	0.95227	0.44802	0.2478	0.12
$M = 7$	1.72781	0.95227	0.44802	0.2485	0.14
$M = 8$	1.72781	0.95227	0.44802	0.2468	0.11
Bloch:	$\arg(\mu_0)$	$\mu_1 \times 10^2$	$\mu_2 \times 10^4$	$\mu_3 \times 10^6$	$\mu_4 \times 10^8$
	1.72781	0.95227	0.44802	0.2494	0.15

TABLE 1. Convergence with increasing M of the eigenvalues, λ_i $(i = 0, 1, 2, 3, 4)$, of the extended transfer matrix, $\mathscr{P}$, to eigenvalues, μ_i $(i = 0, 1, 2, 3, 4)$, of the Bloch problem for elevated sinusoidal topography defined by (5.11) with $b/h_2 = \frac{1}{2}$, $\ell/h_2 = 1$ and $k_2\ell = 1.5$.

yields a homogeneous matrix equation, (5.7), which is Hermitian by construction and in which the alternative eigenvalue parameter $\beta \in \mathbb{R}$ is given numerically by the zeros of a real determinant.

The numerical procedure and the values of the various truncation parameters outlined in the scattering problem are adopted in each of the methods used for solving the Bloch problem.

We have previously demonstrated (see § 4.2) that the eigenvalues $\mu_i(K)$ we now seek coincide with those, λ_i, $(i = 0, \ldots, M)$ of the extended transfer matrix $\mathscr{P}$ arising in the scattering problem, in the the limit $M \to \infty$. This relationship is confirmed numerically in table 1, where the eigenvalues of the Bloch problem are compared for a typical bed shape (see table caption) with the eigenvalues of $\mathscr{P}$, evaluated for increasing values of M. There is very little variation of μ_i with $k_2\ell$, so results are compared for just one value, $k_2\ell = 1.5$. Calculation of the smaller eigenvalues of the matrix $\mathscr{P}$ is extremely sensitive to numerical rounding errors and for this reason only the first four eigenvalues can be compared. In this example, it was necessary to significantly increase with M the truncation parameters used in the numerical scheme (for $M = 8$ values of $S_1 = 24$, $S_2 = 36$, and 2000 evaluations per integral were used) in order to resolve the values of λ_3 and λ_4 to a sufficient accuracy. This is not surprising as the sequence of eigenvalues $\{\lambda_i\}$ decreases to zero very rapidly and the accurate evaluation of the $M + 1$ eigenvalues requires all other factors in the numerical procedure to be determined to at least an equal accuracy. For this reason it is inadvisable to use values larger than $M = 8$ although the value of $|R|$ from the scattering problem does not appear to be affected significantly by errors in the values of the individual eigenvalues.

Also, in figure 9 we show the relationship between $k_2\ell/\pi$ and μ_0 corresponding to the bed shape used in figure 4. The solid curve in figure 9 corresponds to the left-hand scale which shows $\beta\ell = \arg(\mu_0)$, whilst the dashed curve corresponds to $|\mu_0|$ measured against the right-hand scale. Here, and in the following figures, we have chosen to replace $K = \omega^2/g$ as the frequency parameter in these examples with k_2 relating to the wavenumber at the minimum depth, h_2, of the bedform in order to identify relationships with the results from the corresponding scattering problems. Figure 9 confirms that there is at most one complex eigenvalue of the Bloch problem,

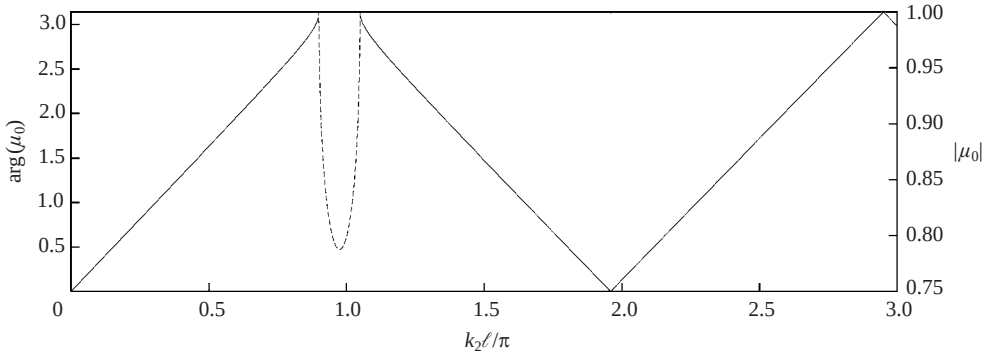

FIGURE 9. Variation of $\beta\ell = \arg(\mu_0)$ (solid curves, left-hand scale) and $|\mu_0|$ (dashed curve, right-hand scale) against $k_2\ell/\pi$ for sinusoidal topography defined in figure 4.

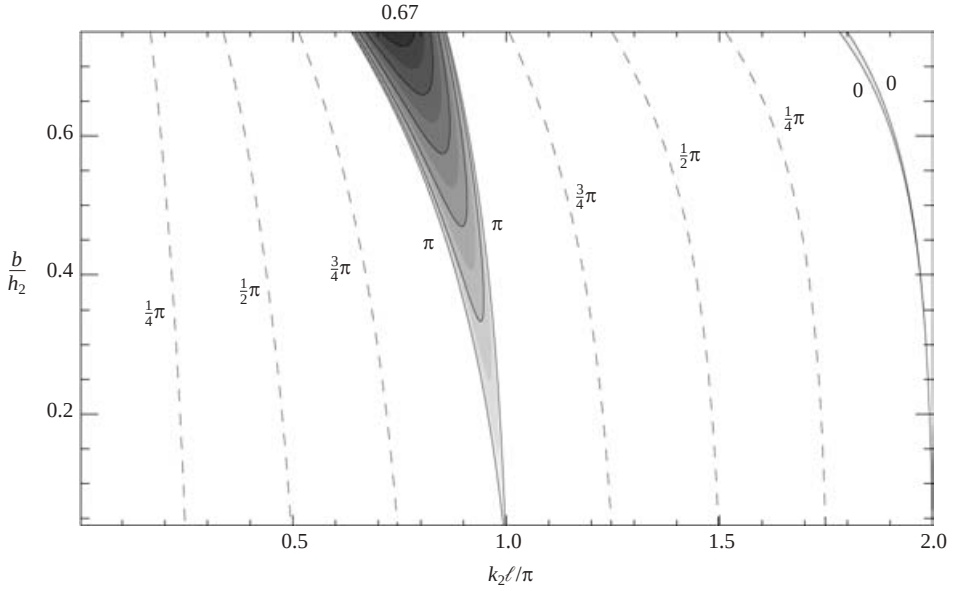

FIGURE 10. Lines showing variation of $k_2(\beta)$ against b/h_2 for values of $\beta\ell = p\pi/4$, $p = 0, \ldots, 4$, (labelled against curves) in the case of a sinusoidal bedform with $\ell/h_2 = 2$. Shaded regions show $|\mu_0| \leqslant 1$.

$\mu_0 = e^{i\beta\ell}$, with $\arg(\mu_0) \in [0, \pi]$ and that there are intervals of k_2 between values of $\beta = \pi$ and $\beta = 0$ where the eigenvalue μ_0 is real (the second and third intervals are too small to show up graphically). In this case curves of the eigenvalue λ_0 of the extended transfer matrix $\mathscr{P}$ for all $M \geqslant 0$ are so close to the curves of μ_0 from the Bloch problem that they have not been included in figure 9. This implies, in this particular example, that $\alpha \approx \beta$, where $e^{\pm i\alpha\ell}$ are the two eigenvalues of $\mathscr{P}$, the transfer matrix for $M = 0$. Other examples also reveal that α is a very good approximation to β.

Two further graphical illustrations of certain features of the solution to the Bloch problem are presented in figures 10 and 11. Here, we concentrate on the relationship between μ_0 and k_2 as the amplitude and length (respectively) of an infinite sinusoidal

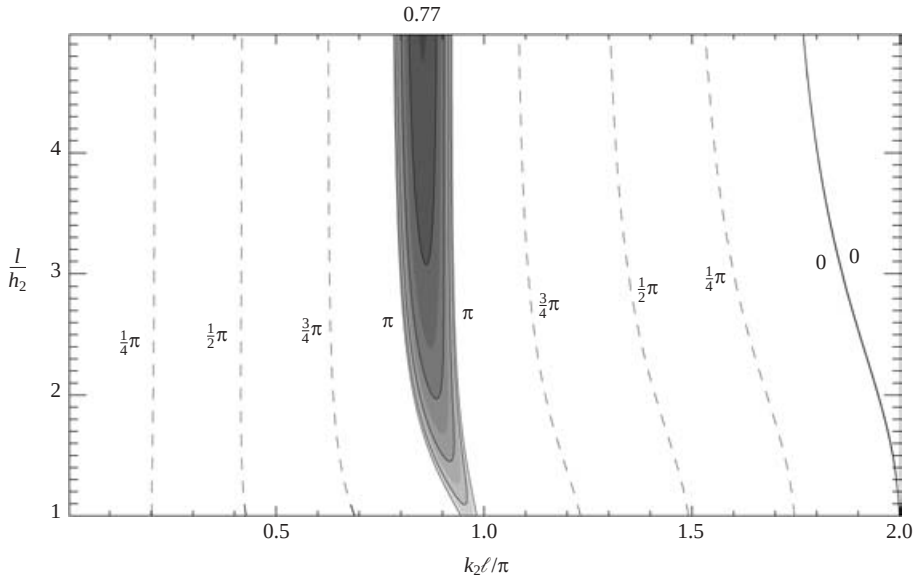

FIGURE 11. Lines showing variation of $k_2(\beta)$ against ℓ/h_2 for values of $\beta\ell = p\pi/4$, $p = 0, \ldots, 4$, (labelled against curves) in the case of a sinusoidal topography with $b/h_2 = \frac{1}{2}$. Shaded regions show $|\mu_0| \leqslant 1$.

topography is varied. This is achieved by showing $k_2(\beta)$ for $\beta = p\pi/4$, $p = 0, 1, 2, 3, 4$ and, in intervals of k_2 where μ_0 is real, shading and showing contour levels of $\mu_0 \leqslant 1$.

Clearly, Bragg resonance in the scattering problem is a direct consequence of the absence of eigenvalues of $\mathscr{P}$ having unit modulus and it is therefore directly related to the absence of complex eigenvalues in the Bloch problem. Therefore, the non-existence of propagating waves over infinite periodic topography implies Bragg resonance in the associated scattering problem over a finite periodic bed, and conversely.

Therefore, the shaded regions of figures 10 and 11 show exactly the intervals where Bragg resonance occurs and where propagating Bloch waves do not exist for a range of sinusoidal topographies. Also the darker the shading, the smaller the value of μ_0, indicating an increase in the magnitude of the reflected wave amplitude. We remark that figures 10 and 11 are counterparts for full linear theory of the stability diagram for the Mathieu equation, which arises in ripple bed scattering using shallow-water theory (see Davies *et al.* 1989).

The bounds on Bragg resonance are given by values of $\beta = 0$ and $\beta = \pi$. However, the Bloch problem is a local problem involving a single period of topography and therefore the interval supporting resonance in the scattering problem is independent of the way in which the finite periodic bed attaches itself to the levels in $x < 0$ and $x > N\ell$. This explains why the curves of R_b in figures 7 and 8, which share the same periodic topography in $0 < x < N\ell$ but are wholly elevated and depressed respectively, pass through $R_b = 1$ at approximately the same values of wavenumber k_2. These values of k_2 are only approximately equal, as R_b is a quantity derived from the $M = 0$ wide-spacing approximation and is determined from quantities arising from the scattering by a single period which in the case of figure 7 is the elevated topography and in the case of figure 8 is the depressed topography.

Sloshing modes for N periods of symmetric topography contained between vertical walls at $x = 0$ and $x = N\ell$ are particular cases of the Bloch problem where $\beta = p\pi/N$,

$p = 0, \ldots, N$, are prescribed values from which the frequency parameter K (or k_2) is sought, as described in § 4.3. Results for the sloshing frequencies over $N = 4$ periods are therefore illustrated by the dashed lines and the solid lines $\beta = \pi$ and $\beta = 0$ in figures 10 and 11 for a range of configurations of sinusoidal topography. Clearly, the sloshing modes for $N = 2$ and $N = 1$ are subsumed into those for $N = 4$. The streamline patterns for the first few sloshing modes for $N = 2$ periods are shown in figure 1 and the frequencies at which they occur may be determined from $l/h_2 = 1$ in figure 11 for $\beta = 0, \pi/2, \pi$.

In particular, the sloshing modes over a single period of topography, given by the values of $\beta = 0$ and $\beta = \pi$, are precisely the bounds on Bragg resonance in the corresponding scattering problem involving an arbitrary number of periods of connected topography. For example, the frequencies of the two sloshing modes given in figures 1(*c*) and 1(*d*) bound the interval of Bragg resonance for a sinusoidal periodic bed with $b/h_2 = \frac{1}{2}$ and $\ell/h_2 = 1$. Previous estimates for the location and width of the interval of Bragg resonance have been limited to approximations based on small bed elevations. Not only can this interval be now given exactly, but the mechanism by which it occurs has also been revealed.

In the all cases of scattering by bedforms possessing symmetry (that is, all except the case in figure 6) we have observed that zeros of reflection occur at regular wavenumber intervals. These are explained in terms of the wide-spacing formula for $|T|$ in (3.24) which predicts $R = 0$ at $\alpha = p\pi/N$ for integer values of p. This observation has also been recorded by Evans (1990) in a related study based entirely on wide-spacing methods. Since α is the $M = 0$ approximation to β, we may therefore deduce that values of $k_2(\beta)$ for $\beta = p\pi/N$, $p = 1, \ldots, N-1$, and not including $p = 0$ or $p = N$ – equivalent to sloshing modes over N periods in a tank – are also approximations to wavenumbers at which zeros of reflection occur. The correspondence between properties of the sloshing problems and the scattering problem has been made for symmetrical topography only, and could explain the non-vanishing local minima of R observed in figure 6 for the doubly periodic sinusoidal topography which lacks symmetry.

6. Conclusions

We have used integral equation techniques to solve and relate three water wave problems involving periodic bedforms. The main features of the work may be summarized as follows.

A transfer matrix approach has been devised for scattering, which incorporates an arbitrary number of evanescent modes. For a single period of the bed, the method gives the full linear solution to any accuracy, irrespective of the number, M, of evanescent modes included in the transfer matrix. The value of M is determined numerically, by requiring that the solution of the scattering problem for an ensemble of N contiguous periods, obtained by coupling N transfer matrices, has a given accuracy. We thus obtain the exact solution for ripple bed scattering, on the basis of full linear theory, with which we have compared previous approximations derived by using the modified mild-slope equation. The transfer matrix formulation can be applied to scattering by any topography, without incurring errors such as those that arise from bed discretization. In particular, the approach could be used to examine scattering by random periodic beds.

In parallel with the solution method devised for the scattering problem, we have proposed an extended Bloch problem, which includes the conventional formulation

for waves propagating over an infinite periodic bed. It has been shown that the eigenvalues of the scattering transfer matrix corresponding to the inclusion of M evanescent modes and the eigenvalues of the extended Bloch problem coincide as $M \to \infty$. This connection allows the solution of the scattering problem for N ripples to be deduced entirely from the solution of the Bloch problem, and conversely. The problem of sloshing frequencies and modes has been examined via the Bloch problem.

The relationships between the three problems imply, in particular, that the frequency bands supporting the existence of Bragg resonance in the scattering context are bounded by sloshing frequencies and correspond to the non-existence of propagating Bloch waves. These bands are approximated well by the envelope of the reflection coefficients given by the wide-spacing approximation, in which no evanescent modes occur in the coupling between adjacent periods. The connections between the problems is summarized in figures 10 and 11, which are reminiscent of "stability diagrams" arising in the theory of ordinary differential equations with periodic coefficients.

A robust set of numerical methods has been developed and exhaustively tested. These have been used to produce results that confirm and illustrate the principal features of the theory, a selection of which is given above. It should be remarked that, because the eigenvalues of the transfer matrix have widely differing magnitudes (resulting from their occurrence in reciprocal pairs), they are not easy to determine numerically. We have obtained sufficient eigenvalues to fulfil the immediate objectives of the present work, but a further investigation of the numerical approach would be needed prior to increasing the value of M significantly.

The authors would like to thank Dr Peter Chamberlain of the Mathematics Department, University of Reading for producing the results based on the modified mild-slope equation.

REFERENCES

Ashcroft, N. W. & Mermin, N. D. 1976 *Solid State Physics.* W. B. Saunders, Philadelphia.

Berkhoff, J. C. W. 1973 Computation of combined refraction-diffraction. *Proc. 13th Conf. on Coastal Engng, July 1972, Vancouver, Canada*, vol. 2, pp. 471–490. ASCE.

Berkhoff, J. C. W. 1976 Mathematical models for simple harmonic linear waves. Wave diffraction and refraction. *Delft Hydr. Rep.* W 154-IV.

Chamberlain, P. G. & Porter, D. 1995*a* The modified mild-slope equation. *J. Fluid Mech.* **291**, 393–407.

Chamberlain, P. G. & Porter, D. 1995*b* Decomposition methods for wave scattering by topography with application to ripple beds *Wave Motion* **22**, 201–214.

Chou, T. 1998 Band structure of surface flexural-gravity waves along periodic interfaces. *J. Fluid. Mech.* **369**, 333–350.

Collin, R. E. 1991 *Field Theory of Guided Waves*, 2nd Edn. IEEE Press; Oxford University Press.

Davies, A. G. 1982 The reflection of wave energy by undulations on the seabed. *Dyn. Atmos. Oceans* **6**, 207–232.

Davies, A. G., Guazzelli, E. & Belzons, M. 1989 The propagation of long waves over an undulating bed. *Phys. Fluids* A **1**, 1331–1340.

Davies, A. G. & Heathershaw, A. D. 1984 Surface-wave propagation over sinusoidally varying topography. *J. Fluid Mech.* **144**, 419–443.

Devillard, P., Dunlop, F. & Souillard, B. 1988 Localization of gravity waves on a channel with a random bottom. *J. Fluid Mech.* **186**, 521–538.

Evans, D. V. 1990 The wide-spacing approximation applied to multiple scattering and sloshing problems. *J. Fluid Mech.* **210**, 647–658.

Guazzelli, E., Rey, V. & Belzons, M. 1992 Higher-order Bragg reflection of gravity surface waves by periodic beds. *J. Fluid Mech.* **245**, 301–317.

KIRBY, J. T. 1986 A general wave equation for waves over rippled beds. *J. Fluid Mech.* **162**, 171–186.

KREISEL, G. 1949 Surface waves. *Q. Appl. Maths* **7**, 21.

MCIVER, P. 2001 Water-wave propagation through an infinite array of cylindrical structures. *J. Fluid. Mech.* **424**, 101–125.

MASSEL, S. R. 1993 Extended refraction-diffraction equation for surface waves. *Coastal Engng* **19**, 97–126.

MEI, C. C. 1985 Resonant reflection of surface water waves by periodic sandbars. *J. Fluid Mech.* **152**, 315–335.

MILES, J. 1998 On gravity-wave scattering by non-secular changes in depth. *J. Fluid Mech.* **376**, 53–60.

O'HARE, T. J. & DAVIES, A. G. 1992 A new model for surface wave propagation over undulating topography. *Coastal Engng* **18**, 251–266.

O'HARE, T. J. & DAVIES, A. G. 1993 A comparison of two models for surface-wave propagation over rapidly-varying topography. *Appl. Ocean Res.* **15**, 1–11.

PORTER, R. & EVANS, D. V. 1999 Rayleigh-Bloch surface waves along periodic gratings and their connection with trapped modes in waveguides. *J. Fluid Mech.* **386**, 233–258.

PORTER, R. & PORTER, D. 2000 Water wave scattering by a step of arbitrary profile. *J. Fluid Mech.* **411**, 131–164.

REY, V. 1992 Propagation and local behaviour of normal incident gravity waves over varying topography *Eur. J. Mech.* B: *Fluids* **11**, 213–232.

SMITH, R. & SPRINKS, T. 1975 Scattering of surface waves by a conical island. *J. Fluid Mech.* **72**, 373–384.